RESEARCH ARTICLE

Key Points:

- Photosensitized manganese (Mn) aerosols may be important heterogeneous drivers for isoprene oxidation in the atmosphere
- Surface-enhanced heterogeneous reactions facilitate the generation and release of singlet oxygen (O(^{1}D)) and hydroxyl (OH) radicals
- Low-molecular-weight carbonyls can be major products of isoprene oxidation, becoming dominant in the aging process of organic aerosols

Author Contributions:

Conceptualization: Hong Liao, Junji Cao, Shun-cheng Lee, Xinlei Ge, Yu Huang
Data curation: Jingyi Li, Yunjiang Zhang, Junfeng Wang, Hongli Wang, Cheng Huang, Qingyan Fu, Xinlei Ge, Yu Huang, Judith C. Chow, John G. Watson
Formal analysis: Haiwei Li, Jingyi Li, Wingkei Ho, Long Cui, Ming Wang, Yunjiang Zhang, Junfeng Wang, Cheng Huang, Qingyan Fu, Yuanchun Jiang, Mindong Chen, Hong Liao, Junji Cao, Shun-cheng Lee, Xinlei Ge, Yu Huang, Judith C. Chow, John G. Watson
Funding acquisition: Haiwei Li, Xinlei Ge

Exploring Surface-Enhanced Heterogeneous Oxidation of Isoprene: Evidence for Atmospheric Haze Chemistry

Haiwei Li[1,2] [ID], **Jingyi Li**[1] [ID], **Wingkei Ho**[3] [ID], **Long Cui**[4] [ID], **Ming Wang**[1], **Yunjiang Zhang**[1] [ID], **Junfeng Wang**[1] [ID], **Hongli Wang**[2] [ID], **Cheng Huang**[2] [ID], **Qingyan Fu**[2] [ID], **Yuanchun Jiang**[1], **Mindong Chen**[1] [ID], **Hong Liao**[1] [ID], **Junji Cao**[5] [ID], **Shun-cheng Lee**[6] [ID], **Xinlei Ge**[1] [ID], **Yu Huang**[4] [ID], **Judith C. Chow**[7] [ID], and **John G. Watson**[7] [ID]

[1]Joint International Research Laboratory of Climate and Environment Change, Jiangsu Key Laboratory of Atmospheric Environment Monitoring and Pollution Control, Collaborative Innovation Center of Atmospheric Environment and Equipment Technology, School of Environmental Science and Engineering, Nanjing University of Information Science and Technology, Nanjing, China, [2]Key Laboratory of Formation and Prevention of Urban Air Pollution Complex, Ministry of Ecology and Environment, Shanghai Academy of Environment Sciences, Shanghai, China, [3]Department of Science and Environmental Studies, The Education University of Hong Kong, Hong Kong, China, [4]State Key Laboratory of Loess and Quaternary Geology (SKLLQG) and Key Laboratory of Aerosol Chemistry and Physics, Institute of Earth Environment, Chinese Academy of Sciences, Xi'an, China, [5]Institute of Atmospheric Physics, Chinese Academy of Sciences, Beijing, China, [6]Sustainable Energy and Environment Thrust, The Hong Kong University of Science and Technology (Guangzhou), Guangzhou, China, [7]Division of Atmospheric Sciences, Desert Research Institute, Reno, NV, USA

Abstract Solid atmospheric particulates can act as heterogeneous drivers for gas loss and particle aging during haze episodes. Observational and experimental evidence reveals an unidentified competitive mechanism involving transition metal ions (TMIs) that catalyze the heterogeneous oxidation of isoprene. Hydroxyl radicals (OH) were generated through the reaction of singlet oxygen (O(^{1}D)) with molecular water at the surface of earth-abundant manganese (Mn) nanoparticles. The energy threshold for OH production was minimized to 213 kJ mol^{-1} in the presence of alkali K$^+$ ions, significantly lower than the 392 kJ mol^{-1} required for ozone photolysis. The rapid loss of isoprene (1.60×10^{-2} s^{-1}) for the particulate mixtures resulted in the formation of approximately 70% C$_1$–C$_4$ carbonyl oligomers via interfacial binding modes, which promoted particle growth. This contrasts with the higher yields of C$_5$ products typically observed in gas-phase reactions of isoprene with OH radicals. The findings could enhance the understanding of severe haze formation, particularly under complex air pollution conditions.

Plain Language Summary Unlike the "London fog" and "Los Angeles smog," which are primarily associated with coal burning and petrol consumption, many developing countries (such as China and India) experience a more complex chemical system due to minimal emission controls. There is a need for interdisciplinary research to elucidate the missing pathways of gas loss and aerosol formation under these complex air pollution conditions. Previous studies have indicated that fine-particle transition-metal-ion (TMI) aerosols, such as manganese (Mn) and iron (Fe), can function as oxidizers, enhancing particulate sulfate production during haze episodes due to their large surface-specific profiles and photosensitive catalytic properties. This work presents observational and experimental evidence of an unidentified mechanism for Mn-catalyzed hydroxyl radical production and the heterogeneous reactions of isoprene. These TMI pathways provide an additional avenue for initiating isoprene oxidation, thereby extending current understanding of atmospheric heterogeneous mechanisms.

1. Introduction

Surface-enhanced heterogeneous chemistry influences atmospheric gas and particulate matter (PM) concentrations (George & Abbatt, 2010; Harris et al., 2013; Kong et al., 2021). Fine-particle transition-metal-ions (TMI) in minerals, such as manganese (Mn) and iron (Fe) compounds, which have aerodynamic diameters in the nanometer range, can act as heterogeneous catalysts for the production of particulate sulfate from sulfur dioxide (SO$_2$) oxidation during haze episodes (Harris et al., 2013; Hochella et al., 2019; Ma et al., 2023; Wang et al., 2021). Previous studies have shown that surface reactions catalyzed by Mn nanoparticles can enhance sulfate formation by approximately 69.2% compared to conventional pathways (Gao et al., 2022; Li et al., 2020; Wang et al., 2021). The Weather Research and Forecasting Model coupled with Chemistry (WRF-Chem) and box models, which

Investigation: Haiwei Li, Jingyi Li, Wingkei Ho, Long Cui, Junfeng Wang, Hongli Wang, Cheng Huang, Qingyan Fu
Methodology: Haiwei Li, Jingyi Li, Hongli Wang, Mindong Chen, Shun-cheng Lee, Xinlei Ge, Yu Huang, Judith C. Chow, John G. Watson
Project administration: Xinlei Ge
Resources: Cheng Huang, Qingyan Fu, Yuanchun Jiang, Mindong Chen, Hong Liao, Junji Cao, Shun-cheng Lee, Xinlei Ge, Yu Huang, Judith C. Chow, John G. Watson
Supervision: Xinlei Ge, Yu Huang, Judith C. Chow
Validation: Wingkei Ho, Long Cui, Ming Wang, Judith C. Chow
Visualization: Jingyi Li, Long Cui, Xinlei Ge, John G. Watson
Writing – original draft: Haiwei Li
Writing – review & editing: Jingyi Li, Wingkei Ho, Long Cui, Ming Wang, Yunjiang Zhang, Junfeng Wang, Hongli Wang, Cheng Huang, Qingyan Fu, Yuanchun Jiang, Mindong Chen, Hong Liao, Junji Cao, Shun-cheng Lee, Xinlei Ge, Yu Huang, Judith C. Chow, John G. Watson

include newly added heterogeneous reactions, suggest that sulfate enhancement occurs through heterogeneous pathways rather than through aqueous-phase reactions initiated by dissolved oxidants such as ozone (O_3), hydrogen peroxide (H_2O_2), and nitrogen dioxide (NO_2) (Song et al., 2021; Wang et al., 2021). However, field measurement and characterization of these heterogeneous processes remain challenging, leading to a scarcity of studies on the interactions between TMI and other reactive gases, resulting in findings that are often rare and ambiguous.

Biogenic isoprene contributes approximately half of the volatile organic compound (VOC) flux, and its degradation (∼85%) is dominated by hydroxyl radical (OH) oxidation (Wennberg et al., 2018). Urban-scale isoprene emissions in US and European cities have been linked to volatile chemical products (VCP) and mobile source emissions. In contrast, over 70% of isoprene emissions in urban China are attributed to industrial VOC sources, potentially leading to different chemical processes (Coggon et al., 2021; He et al., 2022). However, direct evidence for the heterogeneous oxidation of isoprene remains limited. A comprehensive gas-phase oxidation mechanism of isoprene and its major products has been developed (Berndt et al., 2016; Nguyen et al., 2016; Paulot, Crounse, Kjaergaard, Kürten, et al., 2009; Wennberg et al., 2018). The oxidation of isoprene initiated by OH radicals is rooted in organic peroxy radical (RO_2) chemistry. The initial addition of OH to either of the isoprene double bonds produces a significant fraction of isoprene hydroxy peroxy radicals (ISOPOO) (Wennberg et al., 2018). Regardless of the presence of NO_x [nitric oxide (NO) + NO_2], the dynamic nature of the isomer-specific chemistry is evident through the formation and aging of highly oxygenated organic molecules (HOMs) that result from RO_2 reactions with HO_x [OH + hydrogen peroxy radicals (HO_2)] (Berndt et al., 2016; Jaoui et al., 2019; Shen et al., 2022; Wennberg et al., 2018). This process generated C_5 closed-shell hydroxy hydroperoxides (ISOPOOH), which contain at least four oxygen atoms (Berndt et al., 2016; Shen et al., 2022). Among the ISOPOOH isomers, low volatility dihydroxy epoxides (often referred to IEPOX) and dihydroxy dihydroperoxides [$(HO)_2–C_5H_8–(OOH)_2$] represent the dominant (>75%) isoprene oxidized organic molecules (IPOOM), which are potential precursors of secondary organic aerosol (SOA) (Berndt et al., 2016; Paulot, Crounse, Kjaergaard, Kürten, et al., 2009; Xu et al., 2021). Low-molecular-weight oxygenated VOCs (OVOCs), such as $C_1–C_4$ carbonyls, play a minor role in the reactions of ISOPOO with OH (Nguyen et al., 2016; Paulot, Crounse, Kjaergaard, Kürten, et al., 2009, Paulot, Crounse, Kjaergaard, Kroll, et al., 2009), except when there is an increased branching reaction of ISOPOO with NO (Paulot, Crounse, Kjaergaard, Kroll, et al., 2009; Wennberg et al., 2018; Xu et al., 2021). Carbonyls are preferentially produced during the intramolecular decomposition of isoprene hydroxy nitrates under solar irradiation or nocturnal ozonolysis (Edwards et al., 2017; Müller et al., 2014; Wennberg et al., 2018). The conversions of C_5 ISOPOOH to $C_1–C_4$ carbonyls under low-NO_x conditions may occur through surface reactions with metals (Bernhammer et al., 2017; Rivera-Rios et al., 2015; Yuan et al., 2017).

A missing source of OH radicals has been identified as an important factor in the heterogeneous transformation process. This phenomenon has been investigated in the context of TMI-catalyzed oxidation of SO_2 (Chen et al., 2012, 2021; Ma et al., 2023; Wang et al., 2022). Current chemical mechanisms do not fully account for OH production and the associated OH-initiated oxidation reactions in chemically complex environments (Li et al., 2023; Lu et al., 2018). The total OH production rate is approximately the sum of primary sources [such as the photolysis of O_3 and nitrous acid (HONO), as well as the ozonolysis of alkenes] and secondary sources (dominated by reactions involving NO + HO_2 or RO_2 + HO_2). The unknown OH production rate is estimated to be as high as 30 ppb hr^{-1} at noon, three times greater than the known OH production rate. Consequently, modeling results often underestimate observed OH concentrations by factors of 3–5 (Lu et al., 2018). Numerical simulations involving soot and TMI oxides have demonstrated an increase in OH production through the catalytic surface oxidation of H_2O and the reduction of O_2 (He et al., 2022; Zhang et al., 2022). Coemitted alkali metal ions, such as K^+ and Na^+, can further enhance surface reactions that generate reactive oxygen species (ROS) (Bai & Li, 2014; Wang et al., 2017; Xu et al., 2017). The catalytic effects of these cations on TMI surfaces have been shown to facilitate the decomposition of VOCs (Nie et al., 2013; Wang et al., 2017). Further research is needed to determine the extent to which alkali metal components enhance or inhibit TMI pathways (Gao et al., 2022; Urupina et al., 2022; Wang et al., 2022).

Given the distinct physicochemical profiles of TMI particles and their production of ROS (Ma et al., 2023; Xu et al., 2017), TMI-catalyzed isoprene oxidation could represent an additional pathway for gas loss. This hypothesis was explored by integrating field observations, experimental simulations, and a box model analysis. Since manganese (Mn) nanoparticles exhibit enhanced photosensitive catalysis in the presence of alkali metal

ions (Wang & Didier, 2017; Wang et al., 2017; Xu et al., 2017), we tested three different ratios of K^+ to Mn to evaluate the reactivity of surface heterogeneous reactions. Additionally, the steady uptake and conversion of isoprene and IPOOM at multiple binding sites on Mn surfaces were key features of the heterogeneous mechanism that governed the formation of secondary aerosols.

2. Materials and Methods

2.1. Field Measurements

Observations of mass concentrations for fine-particle Mn and K^+ ions, as well as isoprene, methyl vinyl ketone (MVK), and methacrolein (MACR), were conducted at two urban sites: the Pudong Air Quality Monitoring Supersite (31°13′N, 121°32′E) from January 1 to 20, 2016 and the Shanghai Academy of Environmental Sciences (SAES, 31°100′ N,121°25′ E) from December 1 to 8, 2022, in Shanghai. Detailed descriptions of the sampling sites and online measurements can be found in previous field campaigns (Li, Wang, et al., 2019; Zhu et al., 2023). Table S1 in Supporting Information S1 summarizes the hourly variables from the two field campaigns.

2.2. Preparation and Characterization of Mn Nanoparticles

Mn nanoparticles are present in the atmosphere in their oxidized form (Harris et al., 2012, 2013). However, collecting and extracting high concentrations of TMI nanoparticles from PM samples are challenging (Keller et al., 2013). As shown in Table S2 in Supporting Information S1, particle size distribution and number concentrations vary by location. To address this issue, manganese oxides (MnO_x) were prepared and purified, as described in Text S1.1 in Supporting Information S1. The content of K^+, along with the oxidation state of the MnO_x mixtures, was determined using X-ray photoemission spectroscopy (XPS, Thermo ESCALAB 250Xi, USA), as illustrated in Figure S1 and Table S3 in Supporting Information S1. Due to the larger ionic radius of alkali K^+ ions (0.138 nm) than that of Mn^{n+} ions (e.g., Mn^{4+} at 0.053 nm and Mn^{3+} at 0.065 nm) (Figure S2 in Supporting Information S1), MnO_x cannot be internally mixed with K^+. As shown in Table S4 in Supporting Information S1, when K^+ loadings exceeded 6.0% and 7.5% in MnO_x-K mixtures, both the specific surface area and pore size decreased. To investigate the TMI pathways, two different ratios were prepared: MnO_x with 4.5% K^+ and MnO_x with 3.0% K^+), while MnO_x without potassium (MnO_x-0) served as a control. Characterization techniques of the physicochemical profiles are summarized in Table S5 in Supporting Information S1.

2.3. Experimental Simulations of Heterogeneous Oxidation of Isoprene

Characterizing the dynamic and equilibrium conditions in a flow tube reactor for the heterogeneous activity of gas molecules by MnO_x mixtures presents more challenges than conventional chamber simulations of gas-phase reactions involving isoprene (Cao et al., 2020). We evaluated this activity by examining continuous flow gas exposure, complex photosensitive catalysis, extended reagent residence times, and minimal wall loss. The MnO_x-catalytic oxidation of isoprene was conducted in a fixed bed-like photooxidation chamber reactor, as shown in Text S1.2 and Figure S3 in Supporting Information S1. This setup effectively simulates the continuous interaction between gases and the surfaces of solid particles, closely resembling the surface heterogeneous chemistry found in the atmosphere. In addition to replicating ambient conditions such as temperature, relative humidity, and gas composition, the design minimizes wall loss to enhance the accuracy of the interactions between gaseous reactants and reactive nanoparticles. A xenon lamp was employed to simulate solar irradiation for initiating the photochemical reactions. Time-resolved measurements of isoprene oxidation products were obtained using high-resolution proton transfer reaction time-of-flight mass spectrometry (PTR-ToF-MS, IONICON Analytik GmbH, Austria) across three different MnO_x mixtures. Detailed calibration with a gas standard, along with identification of detected ion formulas and information on detection limits, accuracy, and precision, are provided in Text S1.3 and Tables S6–S7 in Supporting Information S1.

2.4. Model Simulations

As detailed in Text S1.4 in Supporting Information S1, the Master Chemical Mechanism (MCM) in its latest version 3.3.1 is a near-explicit chemical mechanism that describes gas-phase VOC chemistry. It includes enhancements for simulating gas-phase isoprene oxidation chemistry, such as the interconversion and isomerization of isoprene peroxy radicals, as well as the chemistry of IEPOX (Rickard et al., 2015). A box model simulation using the MCM was conducted to quantify the yields of major products, including formaldehyde, MVK, MACR,

hydroxymethyl hydroperoxides (HMHP), ISOPBOOH (tertiary ISOPOOH isomers) and IEPOXB (β-IEPOX) [the most abundant ISOPOOH and IEPOX, respectively (Rickard et al., 2015)] from heterogeneous reactions, in comparison to those from gas-phase reactions of isoprene. The model was initialized with 10 ppb of isoprene and 50 ppb of O_3, based on recommendations from the International Union of Pure and Applied Chemistry (IUPAC) recommendations (Wennberg et al., 2018). The reaction rate constant ($k_{het} \approx 1.60 \times 10^{-2}$ s^{-1}) applies to the equilibrium-state isoprene loss for MnO_x mixtures as illustrated in stage 3 of Figure S8 in Supporting Information S1 (Jacob, 2000).

2.5. Determinations of TMI-Catalyzed ROS Production

The production of $^1O_2$ and OH radicals from different MnO_x mixtures was assessed using radical trapping reagents—specifically, 2,2,6,6-Tetramethylpiperidine (TEMP) for $^1O_2$ and 5,5'-dimethyl-1-pyrroline-N-oxide (DMPO) for OH radicals—using an electron spin resonance (ESR) spectrometer (ER200-SRC, Bruker, USA) under simulated solar light irradiation. Additionally, dominant reactive species were confirmed through radical scavenging experiments in the MnO_x-catalytic oxidation of isoprene, as shown in Text S1.5 in Supporting Information S1. The use of furfuryl alcohol (FFA) and tert-butyl alcohol (TBA) as scavengers effectively inhibited the production of $^1O_2$ and OH radicals, respectively (Qu et al., 2022).

Since the production of ROS was activated and varied with excited radiant energy, the energies emitted by different MnO_x mixtures under light irradiation were measured using fluorescence spectroscopy (FluoroMax, Horiba, France). As described in Text S1.5 in Supporting Information S1, the reagent 3'-(p-hydroxyphenyl) fluorescein (HPF) was employed as a probe to detect selective oxidation by OH radicals without interference from O_2, $^1O_2$, H_2O_2, and other species (Chen et al., 2021). HPF generates a bright green fluorophore at 515 nm in the presence of OH radicals. The activation of MnO_x-catalyzed OH production was evaluated by measuring peak fluorescence under different wavelengths. OH yields were estimated based on the baseline (HPF$_{standard}$) and the accumulated areas of the characteristic fluorescent peaks of the MnO_x mixtures.

2.6. Study of Continuous Surface Reactions for Particle Aging

Conventional chamber experiments that analyze particle number concentrations and size distributions in large reactor volumes (~hundreds of m^3) with reduced surface-to-volume ratios are unable to capture the dynamic changes in heterogeneous adsorption, oxidation, and speciation transformation on isoprene-exposed MnO_x mixtures (Chu et al., 2022). To address this limitation, in situ diffuse reflectance infrared Fourier transform spectrometry (DRIFTS) was employed to study the continuous surface reactions occurring within a flow reactor, allowing for a more detailed examination of particle growth and the dynamic processes involved in these reactions, as illustrated in Text S1.6 and Figure S4 in Supporting Information S1.

The continuous formation of IPOOM complexes during surface reactions with MnO_x mixtures correlates with increasing intensities of IR absorption. The secondary aerosol growth can be quantified using a growth factor (GF), estimated by the ratio GF = I_p/I_0, where I_p represents the sum of the intensities of major species derived from IPOOM after a given exposure time, and I_0 denotes the background intensity of MnO_x mixtures in the absence of isoprene. For this investigation, key IPOOM groups were selected based on their significant peaks in the DRIFTS spectra, including carbonyls at 1,680 cm^{-1}, carboxylates at 1,562 and 1,345 cm^{-1}, methyne at 2,840 and 1,380 cm^{-1}, and diene species at 1,120 cm^{-1}.

3. Results and Discussion

3.1. Observational Evidence for TMI-Catalytic Oxidation of Isoprene

As shown in Figure 1, fine-particle Mn, commonly found in $PM_{2.5}$ samples, contributed to isoprene oxidation and its major oxidation products, such as MVK and methacrolein (MACR), during winter haze episodes in Shanghai, a representative Chinese megalopolis. Over 60% of MVK and MACR are produced through isoprene oxidation in both summer and winter (Coggon et al., 2021; Rivera-Rios et al., 2015; Wennberg et al., 2018). The concentrations of Mn exhibited similar temporal variations with those of MVK and MACR, with a particularly strong correlation ($r = 0.90$) observed during the severe winter haze episodes in 2016. Urban-scale atmospheric chemistry is shaped by diverse local emissions and complex chemical reactions (Figure S5 in Supporting Information S1) (Lu et al., 2018; Ma et al., 2023). One critical aspect of this complexity involves the chemistry
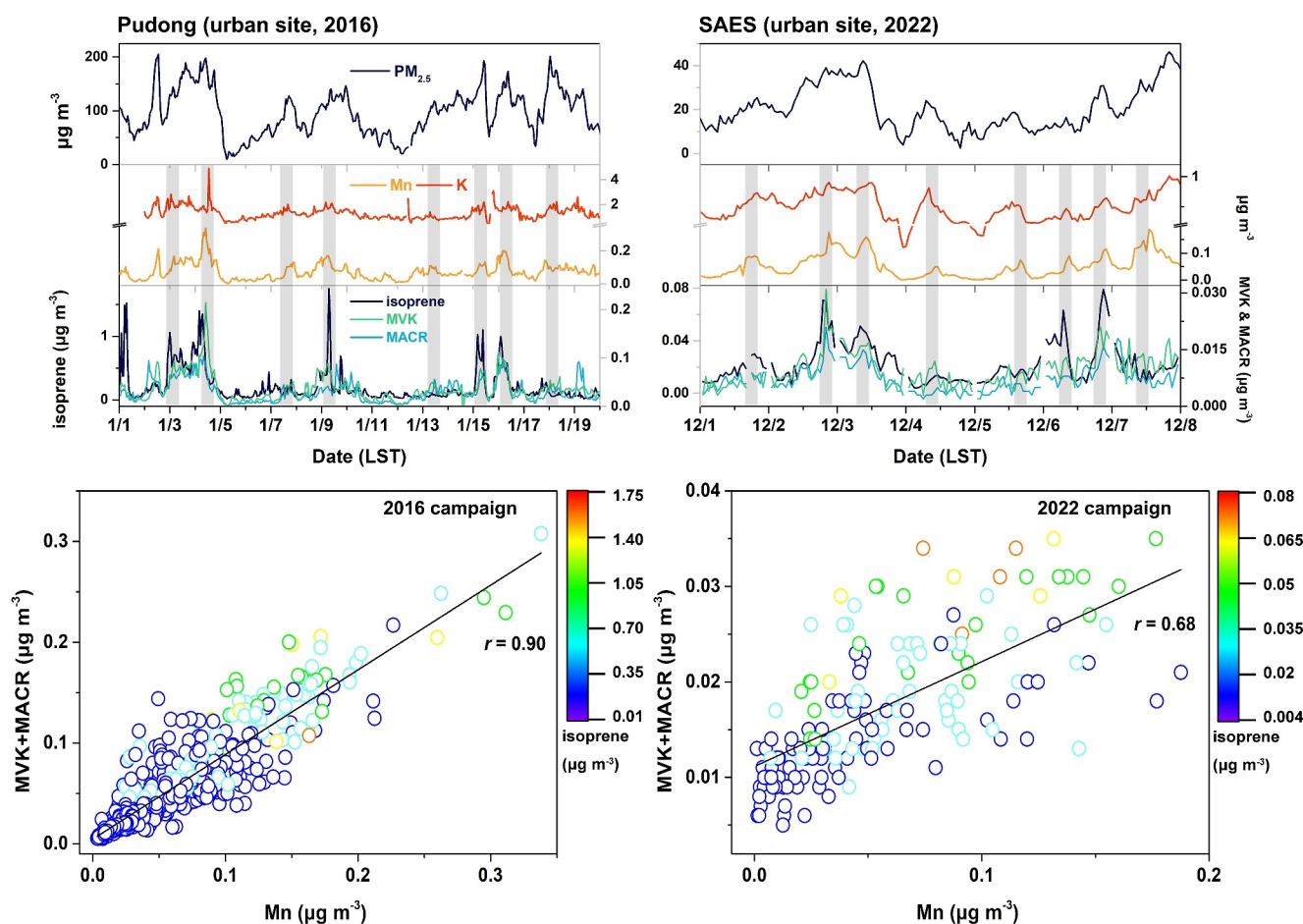
Figure 1. Similar temporal patterns of fine-particle Mn compounds and K^+ ions with first-generation methyl vinyl ketone and MACR from isoprene oxidation observed in the two field campaigns on January 1–20, 2016, and December 1–8, 2022, at two urban sites in Shanghai.

occurring on aerosol surfaces, especially under specific conditions such as urban fuel combustion emissions driving fine-particle pollution, increased humidity, and stagnant air typical of winter haze events. While isoprene is a known marker for biogenic emissions, its urban chemistry may be underestimated if the anthropogenic sources (e.g., VCP, cooking, and building materials) are overlooked (Coggon et al., 2021; Shen et al., 2022). Mn often coexists with Fe (Figure S6 in Supporting Information S1) due to common sources, including soils, non-tailpipe emissions (e.g., tire and brake wear), and fossil fuel combustion (Ma et al., 2023; Wang et al., 2021, 2022). Although Mn constitutes 0.1 wt% (approximately 1.8 mg g^{-1}) of the Earth's crust (Table S8 in Supporting Information S1) (Chen et al., 2012; Harris et al., 2012), Mn nanoparticles produced through combustion processes can achieve high oxidation states, which are characterized by their large surface-to-volume ratios and high thermal stability at ~1,000°C (Quiroz et al., 2015; Wang & Didier, 2017; Xu et al., 2017). In contrast, Fe does not exhibit similar heterogeneous reaction properties, and its catalytic reactions may be inhibited by high ionic strengths (Song et al., 2021; Wang et al., 2021). Mn and Fe have been shown to enhance sulfate formation in Beijing (Figure S7 in Supporting Information S1), contributing to increases of 19.83% and 0.79% during winter and 52.15% and 2.57% during summer, respectively. No significant composite Mn–Fe effects on sulfate formation were observed, likely due to the ease of hydrolysis and low reaction rates of Fe (Wang et al., 2021).

Alkali K^+ ions facilitate Mn-catalyzed isoprene oxidation through interactions between the adsorbate and the sorbent surface, although these interactions remain poorly quantified (Bai & Li, 2014; Wang et al., 2017; Xu et al., 2017). K-promoted TMI catalysis has been shown to be more effective than Na-containing mixtures (Bai & Li, 2014; Urupina et al., 2022). However, elevated concentrations of these cations can inhibit the hydrolysis and dissociation of SO_2, which may consequently reduce sulfate formation (Wang et al., 2022). Despite this potential inhibition, the enhancement of sulfate production during winter remains significant due to TMI catalysis (Li
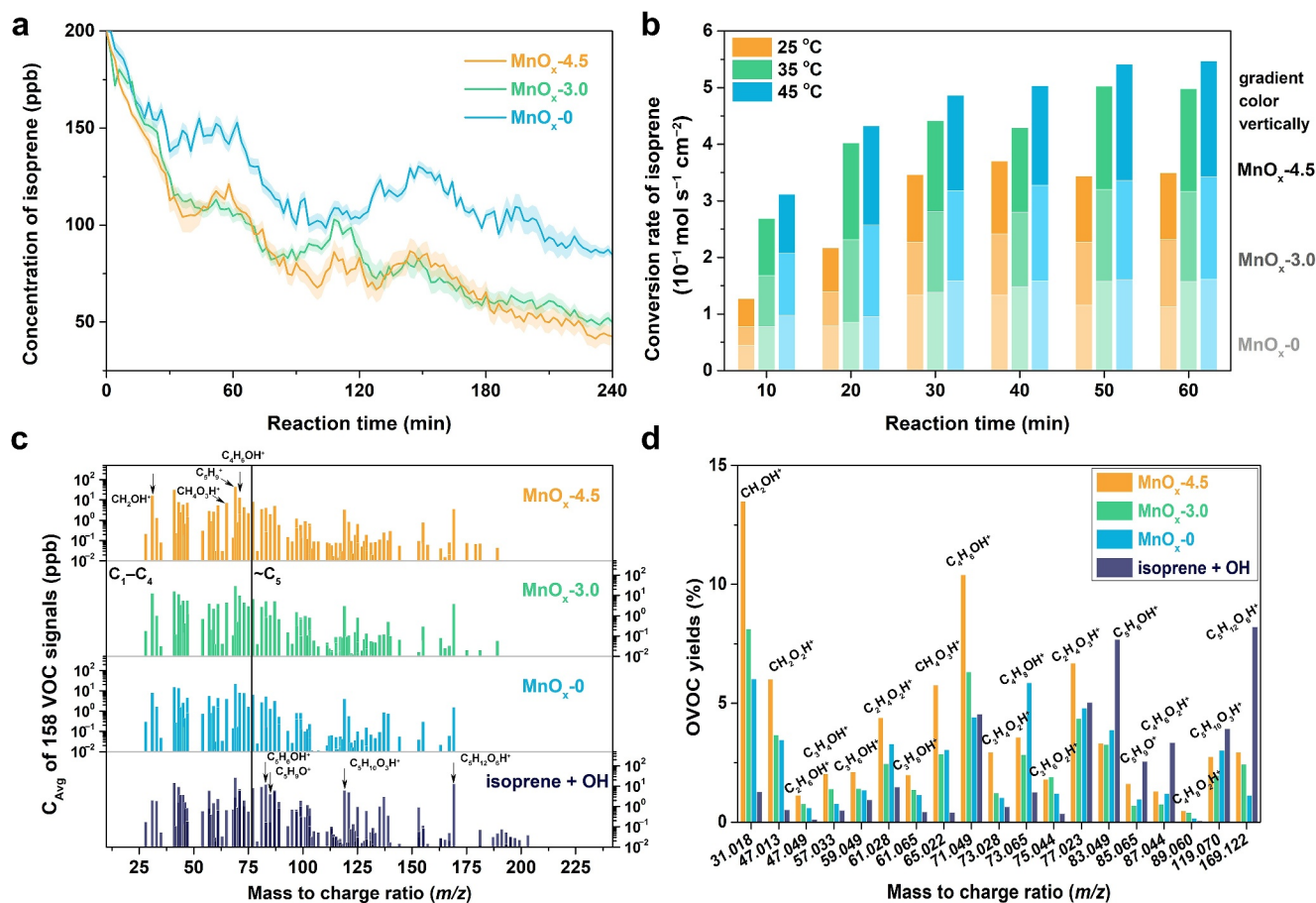
Figure 2. Evolution of heterogeneous oxidation of isoprene (a) and the isoprene conversion rate per unit of specific surface area as a function of reaction time (b) for three different MnO_x mixtures detected by PTR-ToF-MS. Comparisons of the average PTR-MS mass spectrum of isoprene oxidation for MnO_x mixtures with OH-derived isoprene oxidation (background) under UV irradiation (c) and the yields of dominant C_1–C_4 oxygenated compounds (d).

et al., 2020; Wang et al., 2021). While it is unlikely that these findings will reduce uncertainties regarding the activity of TMI mixtures, they provide observational evidence of potential atmospheric chemical pathways, which are explored in the following experimental simulations.

3.2. Laboratory and Modeling Validation of Heterogeneous Activity of Isoprene

Figure 2a shows that isoprene concentrations rapidly decreased by approximately 75% within the first 60 min of irradiation, stabilizing at ~240 min for MnO_x nanoparticles with K^+/MnO_x mass ratios of 4.5% (MnO_x-4.5) and 3.0% (MnO_x-3.0). The process can be divided into three stages (Figure S8 in Supporting Information S1): The initial rapid loss (0–90 min), a slower decline toward equilibrium (90–160 min), and a steady state achieved during stage 3 (160–240 min). In contrast, the decrease was less pronounced for MnO_x-0. Differences among the MnO_x mixtures were less evident in the absence of light irradiation (Figure S9 in Supporting Information S1). Table S4 in Supporting Information S1 shows that surface catalysis was optimized at ~4.5% K^+ mixture, while higher levels of K^+ may lead to a reduction in catalytic activity. This decline can be attributed to the diminishing surface-specific profiles, such as surface area and pore size, which decreased at elevated K^+ loading. However, accurately estimating the heterogeneous activities of atmospheric TMI nanoparticles remains uncertain due to the limited understanding of the active fraction of specific nanoparticles (Hochella et al., 2019; Keller et al., 2013). Given their large surface properties and mass transport capacity, even small amounts of TMI nanoparticles can achieve high-efficiency activity (Liu et al., 2022; Ma et al., 2023). To assess the heterogeneous reaction rates of isoprene as a function of reaction time ($mol_{isoprene} \ s^{-1} \ m^{-2}$, see Equations S1–S2 in Text S1.2 in Supporting Information S1), the rates were normalized by the unit surface area of MnO_x mixtures as isoprene reached

Table 1
Estimates of Reaction Rate for Isoprene Oxidation

Reaction pathways		T (K)	Concentration (molecule cm^{-3})	Rate constant (cm^3 molecule^{-1} s^{-1})	Isoprene loss (s^{-1})	References
Gas-phase reaction (IUPAC recommendation)	isoprene + OH	298	[OH] = 2.0×10^6	1.0×10^{-10} ($2.70 \times 10^{-11} e^{390K/T}$)	2.0×10^{-4}	(Seinfeld and Pandis (2016), Wennberg et al. (2018))
	isoprene + O_3		[O_3] = 1.23×10^{13} (50 ppb)	1.27×10^{-17}	1.56×10^{-4}	
Surface heterogeneous reaction	isoprene + Mn		–	2.40×10^{-16} [a]	1.60×10^{-2} (equilibrium state)	Our recommendation

[a]The rate constant for the catalytic oxidation of isoprene by MnO_x-4.5 was determined based on the conversion rate of isoprene (0.12 mol s^{-1} cm^{-2}, 298K) per unit of specific surface area of MnO_x-4.5 (Table S4 in Supporting Information S1).

equilibrium. The conversion rate has been used to evaluate the activities of surface heterogeneous reactions with gases (Li, Cui, et al., 2019). Isoprene can be oxidized in the atmosphere over a narrow temperature range of 280–315 K (Wennberg et al., 2018); Figure 2b and Table S9 in Supporting Information S1 exhibit the temperature dependence of isoprene conversion rates from 25°C to 45°C, with rates of 0.21 mol s^{-1} cm^{-2} for MnO_x-4.5 and 0.18 mol s^{-1} cm^{-2} for MnO_x-3.0 at 45°C. Similar enhancements in TMI pathways to sulfate formation, ranging from 49.0% to 69.2%, have been linked to temperatures between 5°C and 25°C during winter in northern and eastern China (Li et al., 2020; Wang et al., 2021). Table 1 quantifies the significance of the heterogeneous reaction of isoprene in total isoprene oxidation through kinetics. Oxidation by MnO_x can dominate the loss of isoprene (1.60×10^{-2} s^{-1}, see Figure S8 in Supporting Information S1), which is larger than that by OH (2.0×10^{-4} s^{-1}) and O_3 (1.56×10^{-4} s^{-1}), based on the IUPAC-recommended rate coefficients. This high reactivity helps explain the conversion of isoprene into OVOCs during winter haze episodes. Contrary to the conventional view of PM as a major sink for ROS, the increasing oxidizing power via heterogeneous processes warrants further investigation. The rate coefficient for surface heterogeneous reaction (2.40×10^{-16} cm^3 molecule^{-1} s^{-1}) was measured to be lower than that of the gas-phase reaction of isoprene with OH radicals (1.0×10^{-10} cm^3 molecule^{-1} s^{-1}), indicating that reactions with OH are the dominant sink. Despite the estimated uncertainties for nanoparticles, we advocate for simplified parameterizations that can effectively model this complex chemistry under atmospheric conditions.

Figure 2c shows that C_1–C_4 OVOC products, including formaldehyde (CH_2OH^+, m/z 31.018), MVK + MACR ($C_4H_6OH^+$, m/z 71.049), were dominant in the heterogeneous oxidation of isoprene. In contrast, interactions between OH and ISOPOO lead to subsequent OH-initiated oxidation of C_5 ISOPOOH (Wennberg et al., 2018). Figure S10 in Supporting Information S1 depicts two classic highly oxygenated second-generation organic compounds formed under NO_x-free conditions: IEPOX (HO–C_5H_8(O)–OH) and small dihydroxy dihydroperoxides ((HO)$_2$–C_5H_8–(OOH)$_2$), the first generation of ISOPOOH (Berndt et al., 2016; Paulot, Crounse, Kjaergaard, Kroll, et al., 2009). The background spectrum revealed abundant signals from OH-initiated isoprene oxidation products, recorded without MnO_x mixtures. The formation of IEPOX is indicated by a PTR signal at m/z = 119.070, attributed to $C_5H_{10}O_3$, which signifies the first-generation ISOPOO (Paulot, Crounse, Kjaergaard, Kroll, et al., 2009; Xu et al., 2021; Yuan et al., 2017). Since ISOPOO cannot be directly distinguished in complex gas mixtures, $C_5H_{10}O_3$ fragment ions are surrogates for hydroxy hydroperoxides or the isobaric dihydroxy epoxides (Berndt et al., 2016). Speciated $C_5H_{10}O_3$ is a marker for OH pathways (Berndt et al., 2016; Singh, 2021), with up to 45% of MVK and MACR yields occurring in the presence of NO_x (Wennberg et al., 2018). In the presence of MnO_x mixtures, $C_5H_{10}O_3$ decomposed into carbonyls, aligning with laboratory findings that demonstrate the conversion of ISOPOOH to MVK and MACR through catalytic reactions on metal surfaces (Yuan et al., 2017). As shown in Figure 2d, PTR signals for MnO_x-4.5 indicate strong yields of MVK and MACR, along with formaldehyde. This can be attributed to the generation of carbonyl acylperoxy radicals (R(CO)O_2, a representative of RO_2 radicals), which are related to $C_2H_4O_3H^+$ (m/z 77.023) formed from the reactions of OH radicals with aldehydes or acetones (Rivera-Rios et al., 2015; Wennberg et al., 2018). In addition to further oxidation leading to formate species (e.g., formic acid), the production of formaldehyde from ISOPOO decomposition may be limited by MVK and MACR yields (Nguyen et al., 2016; Vansco et al., 2020). Furthermore, commonly dominant isoprene oxidation products, such as C_5 IEPOX ($C_5H_6OH^+$, m/z 83.049) and ISOPOOH ($C_5H_9O^+$, m/z 85.065), became less influential in heterogeneous oxidation processes. In contrast to

larger molecular weight ISOPOOH [for example, dihydroxy dihydroperoxides ($C_5H_{12}O_6H^+$, m/z 169.122) shown in Figure S11 in Supporting Information S1] (Berndt et al., 2016), coproducts of O_{1-2} OVOCs, such as C_3H_4O, $C_3H_6O_2$, and $C_4H_8O_2$, were abundant in the IPOOM complexes via surface reaction processes (Figure 2d). These ISOPOO products may bond their distal peroxide atoms to the MnO_x surfaces, undergoing prompt decomposition to form C_1–C_4 carbonyls, organic peroxy radicals, and related termination products (such as hydroperoxides), thereby complicating the isoprene oxidation process.

Heterogeneous isoprene oxidation indicates a potential for ozonolysis (Allen et al., 2018; Nguyen et al., 2016). This process generates Criegee intermediates, which are highly reactive carbonyl oxides (R = O^+O^-)* formed from the ozonolysis of terminal alkenes, as shown in Figure S12 in Supporting Information S1 (Nguyen et al., 2016; Welz et al., 2012; Wennberg et al., 2018). While indirect measurements of Criegee intermediates exist, their chemistry in the context of heterogeneous catalytic oxidation of isoprene remains largely unexplored (Bernhammer et al., 2017; Nguyen et al., 2016; Welz et al., 2012; Wennberg et al., 2018). Albeit at lower yields, the presence of HMHP ($HOCH_2OOH$, m/z 65.022) suggests the possible formation of C_1 Criegee upon interaction with MnO_x mixtures, as shown in Figure 2c. This reaction may facilitate the unimolecular decomposition of ISOPOO, further influencing the oxidation pathways of isoprene (Allen et al., 2018; Nguyen et al., 2016; Vansco et al., 2020; Welz et al., 2012). Due to the lack of alkyl substituents, C_1 Criegee cannot adopt a *syn* conformation, resulting in reactive bimolecular reactions with water molecules that produce HMHP, serving as an indicator of Criegee formation (Nguyen et al., 2016). Additionally, four-carbon unsaturated carbonyl oxides, such as MVK oxides (MVK–OO*) and MACR oxides (MACR–OO*), are likely produced during the OH-initiated oxidation of ISOPOO. A small pool of C_1–C_4 Criegee intermediates is presumed to be generated through surface heterogeneous reactions. Further unimolecular or bimolecular reactions involving these intermediates can enhance carbonyl yields for MnO_x mixtures, leading to the formation of vinyl hydroperoxide (VHP) products such as CH_3CHOO, $(CH_3)_2COO$, and CH_3CH_2CHOO (Nguyen et al., 2016). The presence of water vapor, organic acids, and alcohols in the atmosphere can facilitate the isomerization and oligomerization of Criegee intermediates. For instance, formic acid can catalyze the isomerization and adduct formation of isoprene-derived Criegee intermediates at ambient temperatures (Vansco et al., 2020). The MCM was employed using a photochemical box model to simulate the heterogeneous oxidation of isoprene with MnO_x mixtures, compared to the conventional mechanism, as shown in Figure 3 and Tables S10–S11 in Supporting Information S1. The model's incorporation of heterogeneous kinetics suggests that the yields of the C_1–C_4 OVOC pool, including formaldehyde (molar yield of 0.135), MVK + MACR (0.052), HMHP (0.058), and minor IEPOX (0.033), are significantly higher than those resulting from gas-phase reactions of isoprene (Nguyen et al., 2016; Rickard et al., 2015). These modeling results indicate that part of the production of low-molecular-weight OVOCs can be attributed to TMI pathways.

3.3. TMI-Catalyzed ROS Production

Quantifying the effects of surface OH radicals remains uncertain due to challenges in directly measuring heterogeneous reactions of gas molecules (Nosaka et al., 2017). As noted in Section 2.5 above, the determination of surface ROS has been achieved using ESR spectroscopy, which involves adding specific reagents (e.g., TEMP and DMPO) or scavengers (e.g., FFA and TBA) to estimate TMI-catalyzed ROS kinetics (Manfrin et al., 2019; Qu et al., 2022; Zhang et al., 2022). The ESR signals display three characteristic peaks corresponding to TEMP–$^1O_2$ at an intensity ratio of 1:1:1 (Figure 4a), while DMPO–OH exhibited four characteristic peaks at an intensity ratio of approximately 1:2:2:1 (Figure 4b) (Qu et al., 2022). Stronger ESR signals of $^1O_2$ and OH radicals were observed for MnO_x-4.5 and MnO_x-3.0 than MnO_x-0. As shown in Figure 4c, radical scavenging experiments confirmed the presence of two dominant free radicals (Manfrin et al., 2019; Qu et al., 2022). In the absence of radical scavengers, isoprene removal efficiencies were approximately 86% for MnO_x-4.5% and 78% for MnO_x-3.0, compared to 68% for MnO_x-0. The introduction of radical scavengers significantly hindered the catalytic activities of the MnO_x mixtures. Specifically, isoprene removal efficiencies decreased by ∼50% within 10 min following the addition of the $^1O_2$ scavenger, FFA. In contrast, the introduction of the OH scavenger, TBA, did not significantly impact the oxidation activities. This reduction in efficiency suggests that the presence of the $^1O_2$ scavenger quenched the key oxidizing species on the MnO_x surfaces, inhibiting the heterogeneous oxidation process. The results indicate that the oxidation of isoprene and the generation of OH radicals are initiated by reactions involving $^1O_2$. Although $^1O_2$ has a lower oxidizing potential than OH radicals, it exists at higher steady-state concentrations (Manfrin et al., 2019; Seinfeld & Pandis, 2016). These findings underscore the importance of
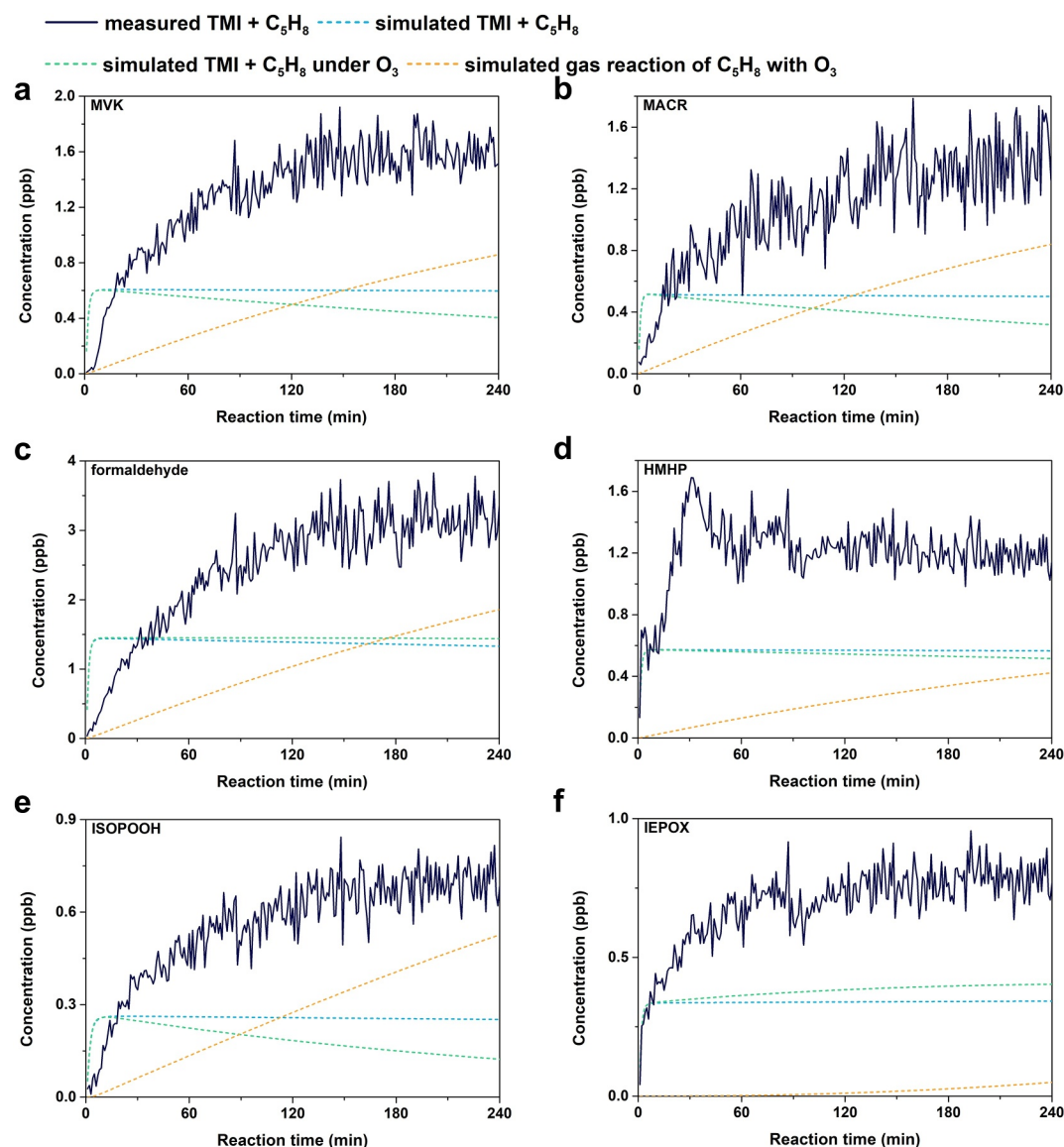
Figure 3. Model calculations of yields of the major isoprene oxidation products, that is, methyl vinyl ketone (a), MACR (b), formaldehyde (c), HMHP (d), ISOPOOH (e), and IEPOX (f) in TMI-catalytic heterogeneous reaction (dash line) incorporated into the Master Chemical Mechanism simulations as compared to the experimentally measured concentrations (solid line).

$^1O_2$ radicals as excited species that act as precursors for OH radicals in surface heterogeneous chemistry. Recent studies have linked surface OH radicals to photosensitive soot particles (He et al., 2022; Zhang et al., 2022). Soot particles from anthropogenic combustion sources may be coated or internally mixed with nanosized TMI oxides, as indicated by XPS analysis (Figure S13 in Supporting Information S1). The enhancement in light absorption, water uptake, and photocatalytic activity of soot particles is partially attributed to the dispersion of abundant TMI oxides. Consequently, TMI-catalyzed isoprene oxidation could also be associated with OH production, which remains underestimated in atmospheric contexts (Chen et al., 2012; Hochella et al., 2019; Wang et al., 2015).

The production of atmospheric $^1O_2$ and OH radicals is limited to the absorption of UV photons that can radiate high excitation energies (Seinfeld & Pandis, 2016). To further investigate the TMI-catalyzed ROS production, we examined the radiant energies for the photoinduced excitation of molecular oxygen by fluorescence spectroscopy (Figures 4d and 4e). Weak fluorescence was observed at 514 nm after selective oxidation of HPF by OH radicals. The TMI-catalyzed OH production showed increased fluorescence at peaks between 544 and 562 nm for MnO_x
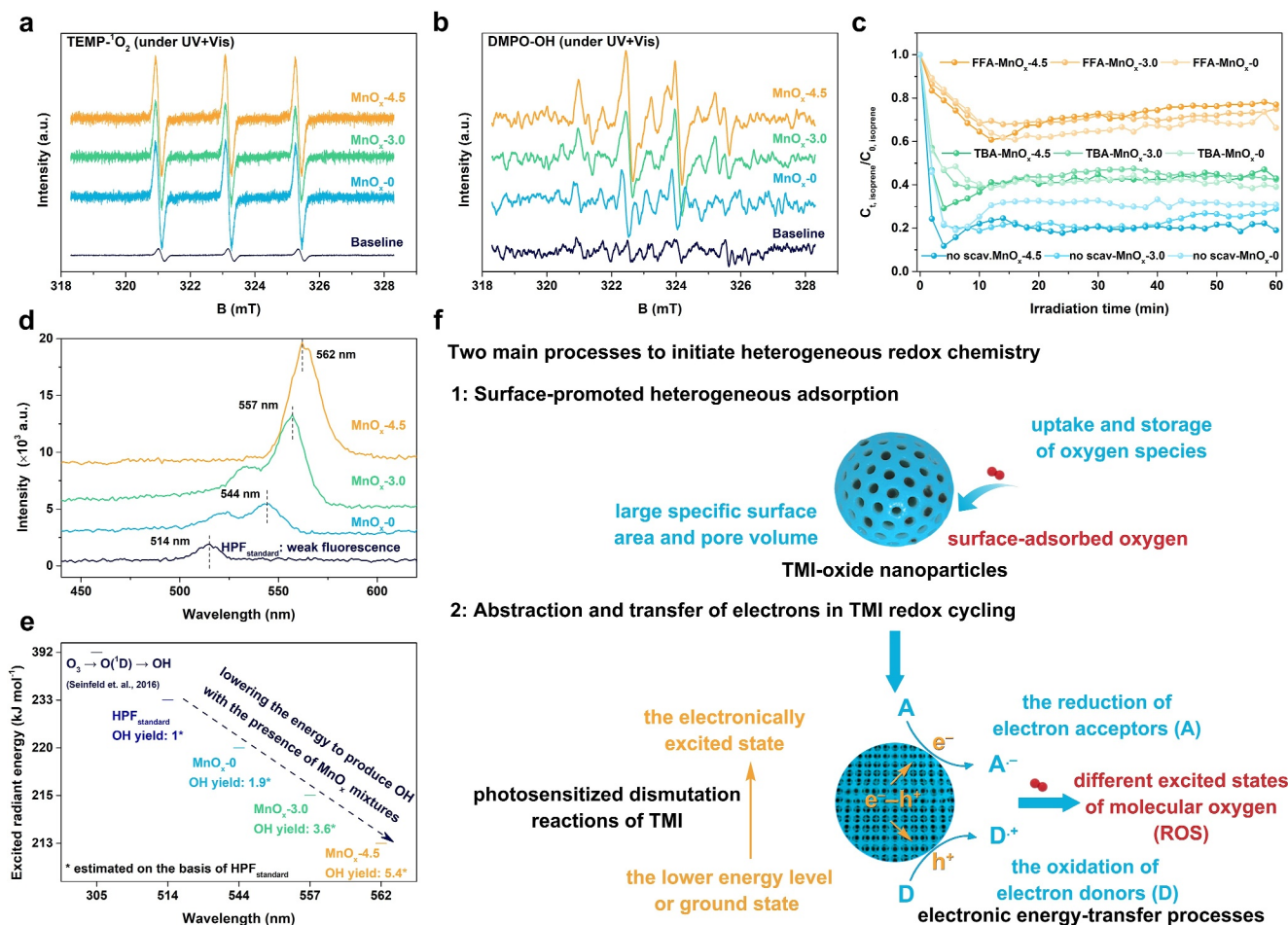
Figure 4. Comparisons in spin-trap electron spin resonance spectra for determination of the first electronically excited state of the oxygen atom O (^{1}D) (singlet oxygen, ^{1}O$_2$ of the molecular formula) (a) and OH radicals (b) activated by MnO$_x$-4.5, MnO$_x$-3.0, and MnO$_x$-0 under light irradiation. Radical quenching experiments using different scavengers (FFA → ^{1}O$_2$ and tert-butyl alcohol → OH) in the heterogeneous oxidation of isoprene (c). Fluorescence spectra of the TMI-catalyzed OH production (d). The excited radiant energy for the OH production negatively correlated with the corresponding wavelength of radiation (e). Diagram of the TMI-catalyzed reactive oxygen species production via photoinduced excitation of oxygen species concerning surface-specific profiles and dismutation reactions of transition metal ion (f).

mixtures. The interaction of ^{1}O$_2$ with unreactive H$_2$O to generate OH requires an excited energy of 392 kJ mol^{-1}, corresponding to approximately 310 nm wavelength radiation (Seinfeld & Pandis, 2016). This energy is significantly higher than the threshold energy of 213 kJ mol^{-1} required for OH radical production from MnO$_x$-4.5, equivalent to an emitted radiation wavelength of 562 nm. Compared to OH yields via gas-phase reaction routes (e.g., O$_3$ photolysis), the radiant energy for OH generation with MnO$_x$ mixtures was achieved under solar visible irradiation. Photosensitive MnO$_x$ catalysis provided additional vibrational (stretching) energy necessary to excite molecular oxygen (Bai & Li, 2014). However, the excited radiant energy does not allow for quantification of OH yields on solid particles. Relative to the baseline (HPF$_{standard}$), OH yields increased by factors of 5.4, 3.6, and 1.9 for MnO$_x$-4.5, MnO$_x$-3.0, and MnO$_x$-0, respectively (Figure 4e).

Figure 4f illustrates the two key processes that initiate surface heterogeneous redox chemistry: (a) surface-enhanced heterogeneous adsorption and (b) the abstraction and transfer of electrons in TMI redox cycling. The monodisperse size distribution shown in Figures S14–S15 in Supporting Information S1 indicates a mean diameter of 50–120 nm for the MnO$_x$ mixtures, which possess a specific surface area and microporosity approximately two orders of magnitude larger than those of PM$_{2.5}$ (Table S4 in Supporting Information S1). Given that soot and TMI particles can exhibit large specific surface areas (~100 m^2 g^{-1}), hydrophilicity, and light absorption coefficients, they can be excited under solar irradiation to initiate efficient heterogeneous catalysis (Liu et al., 2022; Ma et al., 2023). These surface-specific profiles extend isoprene reaction times and facilitate the

adsorption of multiple oxidation products (Wang et al., 2015). Subsequently, interfacial redox reactions are governed by the recycling electron transfers between the oxidation states of transition metals, specifically through the dismutation reactions of TMI (Quiroz et al., 2015), as shown in Figures S16–S17 in Supporting Information S1. An increased Mn content in mixed oxides may enhance these dismutation reactions, contributing to catalytic soot aging (Xu et al., 2017). When radiant energy meets or exceeds the electronically excited energy of TMI, free electrons (e^-) from transition-metal atoms in a lower energy state can transition to an excited state (Figure S18 in Supporting Information S1). Concurrently, holes (h^+) are generated at the lower energy level, facilitating the reduction of electron acceptors (A) by electrons and the oxidation of electron donors (D) by holes (Chen et al., 2012; Ndour et al., 2009; Seinfeld & Pandis, 2016). The activation pathways for key oxidizing species are elaborated in Text S2 in Supporting Information S1. The interfacial redox processes, driven by photosensitive Mn dismutation reactions, are a prerequisite for the formation of O (^{1}D). This process follows two pathways for surface OH generation: (a) $^1O_2$ interacts with H_2O to produce two OH radicals ($^1O_2 + H_2O \rightarrow 2$ OH radicals) (Seinfeld & Pandis, 2016) and (b) photogenerated h^+ reacts with H_2O to produce one OH radical ($h^+ + H_2O \rightarrow$ OH radical + H^+) (Chen et al., 2012). Since surface-adsorbed hydroxyl groups and nitrate ions typically scavenge h^+ produced at the lower electronic states of TMI (Chen et al., 2012; Ndour et al., 2009), the addition of K^+ can enhance the photosensitive Mn dismutation reactions, generating e^-–h^+ pairs and facilitating the breaking of the H–O bond in water to promote the generation of OH radicals (Bai & Li, 2014; Wang et al., 2017, 2022). The pathways involving TMIs remain uncertain due to a lack of direct field measurements. However, the higher isoprene conversion rates observed with MnO_x-4.5 and MnO_x-3.0 illustrate these phenomena. Therefore, the generation and release of surface OH radicals represent complex photosensitized electronic energy transfer processes among different excited states of molecular oxygen (Hochella et al., 2019; Nosaka et al., 2017; Schweitzer & Schmidt, 2003).

3.4. Interfacial Binding Modes of IPOOM and Nanoparticle Growth

In addition to OH oxidation, the potential binding modes of surface-bound species on MnO_x surfaces can prolong the steady adsorption and decomposition of isoprene. In situ DRIFTS measurements were conducted to investigate the intermolecular reactions between IPOOM and MnO_x mixtures through various interfacial binding modes. Figure 5a–5c shows similar IR absorption patterns for the three MnO_x mixtures. As detailed in Table S12 in Supporting Information S1, the IR band observed at 1,120–1,000 cm^{-1} is associated with the diene groups of isoprene (Chu et al., 2019; Yu-Te et al., 2013). The highest intensities of the isoprene absorption peaks were recorded for MnO_x-4.5 and MnO_x-3.0, attributed to their larger surface area and microporosity. The IR spectra indicate the formation of carboxylate groups, with peaks at ~1,562 cm^{-1} for the asymmetrical stretching vibration (v_{as}) of COO–, at 1,345 cm^{-1} for the symmetrical stretching vibration (v_s) of COO–, and at 2,840 and 1,380 cm^{-1} for methyne (–CH). Consistent with the results in Figures 2c and 2d, MnO_x-4.5 shows relatively high adsorption intensities for multiple low-molecular-weight oxidation products of isoprene, including formate, acetate, and carboxylate species. This indicates significant organic uptake by the nanoparticles through surface reactions.

Surface-bound species that react with TMI through multiple interfacial binding modes can undergo isometric isomerization and bond cleavage (Chen et al., 2021; Durand et al., 2010). The splitting of asymmetric and symmetric COO– is commonly used to identify the binding modes of species bound to MnO_x surfaces (Durand et al., 2010). A frequency split (in cm^{-1}) between the v_{as} (COO–) and v_s (COO–) greater than 220 cm^{-1} indicates a monodentate binding mode, while splits similar to or less than 220 cm^{-1} are assigned to a bidentate mode. The observed split of approximately 217 cm^{-1} between 1,562 cm^{-1} and 1,345 cm^{-1} for MnO_x mixtures (Figure 5a–5c) suggests that the surface-bound IPOOM is predominantly bidentate, coexisting with minor monodentate species due to oxygen (O_2) addition, as illustrated in Figure 5d. ISOPOO represents the first generation of isoprene RO_2 radicals formed through OH-initiated oxidation. While the isomerization of ISOPOO cannot be entirely ruled out in the isoprene + OH pathway, theoretical and experimental evidence indicates that most additions occur at the terminal (primary) carbons (Wennberg et al., 2018). The 1-OH addition ISOPOO accounts for approximately 60% of the isomer distribution and is important for elucidating the binding modes of IPOOM interacting with TMI (Seinfeld & Pandis, 2016; Wennberg et al., 2018). In addition to the kinetics of ISOPOO conversion, which are constrained under NO_x-dominated conditions (Paulot, Crounse, Kjaergaard, Kroll, et al., 2009), the production and decomposition of ISOPOO and its adducts are influenced by the interfacial binding modes of O_2 addition with MnO_x mixtures. The reversibility of O_2 addition to ISOPOO bound at metal sites may limit the stabilization of ISOPOOH, thereby facilitating carbonyl formation. Consequently, low-
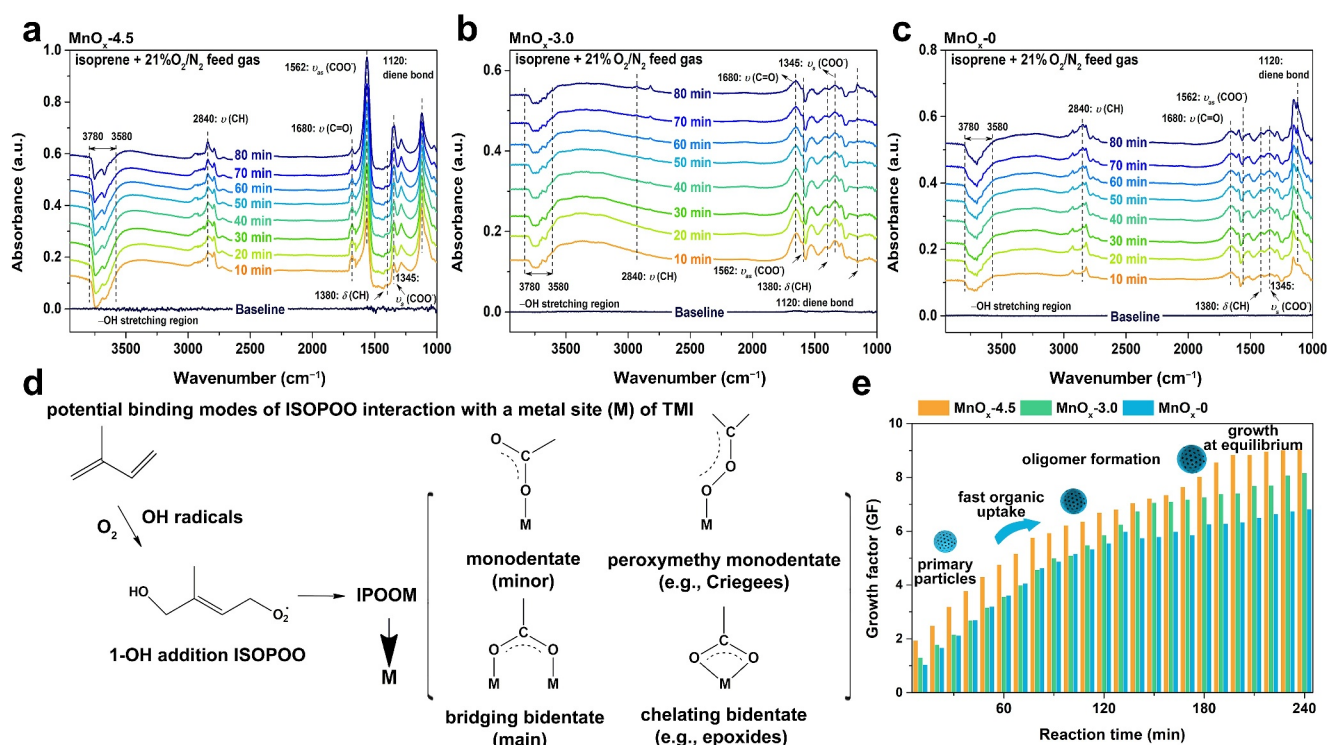
Figure 5. Dynamic changes in in situ diffuse reflectance infrared Fourier transform spectrometry (DRIFTS) spectra of heterogeneous adsorption, oxidation, and transformation over isoprene-exposed MnO_x-4.5 (a), MnO_x-3.0 (b), and MnO_x-0 (c). Potential binding structure and configuration of the IPOOM bound to MnO_x surfaces for the uptake and conversion of isoprene and its oxidation products (d). Estimates of the growth factor of MnO_x nanoparticles interacted with major IPOOM products (including carbonyl at 1,680 cm^{-1}, carboxylate at 1,562 and 1,345 cm^{-1}, methyne at 2,840, and 1,380 cm^{-1}, diene species at 1,120 cm^{-1} observed in the DRIFTS spectra) (e).

molecular-weight carbonyl oligomers at MnO_x surfaces predominantly exhibit a bidentate character with chelating and bridging configurations, while minor peroxy biradicals, such as Criegee intermediates, demonstrate a monodentate mode (Durand et al., 2010; Wennberg et al., 2018). The peroxymethy monodentate mode of COO– coordination is believed to involve a single O–O bond in CH_2OO Criegee intermediates (Li, Cui, et al., 2019; Welz et al., 2012; Yu-Te et al., 2013). The longer O–O bond (~1.35 Å) is reportedly more favorable for dissociative adsorption on metal sites, with a steady state at approximately 4.1×10^3 s^{-1}, compared to the C–O bond (~1.28 Å) (Li, Cui, et al., 2019; Yu-Te et al., 2013). A chelating bidentate binding mode is assumed to be associated with the asymmetric isomerization or thermal dissociation of COO– from potential epoxides. This is supported by the formation of minor C_1 dioxirane (the simplest epoxide) from the isomerization of CH_2OO oxidation by MnO_x (Li, Cui, et al., 2019). The formation of epoxides, such as IEPOX, from the OH-initiated conversion of ISOPOOH is a dominant pathway in atmospheric isoprene oxidation (Berndt et al., 2016; Xu et al., 2021).

The heterogeneous oxidation of isoprene is influenced by surface-adsorbed –OH (Franco et al., 2021; McFiggans et al., 2019), which can act as a precursor of OH radicals and provide additional reaction sites for reactants (Chen et al., 2012). The troughs between 3,780 and 3,580 cm^{-1} in IR spectra are attributed to –OH groups bonded to the metal sites of MnO_x (Li, Cui, et al., 2019; Wang et al., 2015). As $^1O_2$ and OH radicals are generated to oxidize the adsorbed species, the –OH groups are gradually consumed with the MnO_x mixtures. The trough-like patterns of –OH in the IR spectra indicate its progressive consumption during the formation of IPOOM, many of which include carbonyl functionalities (Wennberg et al., 2018). OH radicals can decompose isoprene, resulting in the formation of carboxylates that exhibit features characteristic of RO_2 radicals. Subsequent reactions contribute to the formation of hydroperoxides in the presence of –OH (Bernhammer et al., 2017; Franco et al., 2021). The increased intensity of the –OH suggests a gradual accumulation of surface hydroxyl groups, indicating that –OH plays a role in radical propagation cycles (Wennberg et al., 2018). Although –OH can be partially recycled through O–H dissociation of carbonyl species and water molecules catalyzed by TMI oxides (Jia et al., 2018), $^1O_2$

processes more energy than ground state oxygen atoms and can break the H–O bond in H_2O to produce –OH (He et al., 2022; Seinfeld & Pandis, 2016; Wang et al., 2015). Given that multifunctional products can arise from isoprene oxidation, the catalytic oxidation by TMI was confirmed through surface reactions involving formaldehyde (a highly reactive carbonyl) with MnO_x-4.5 (Figure S19 in Supporting Information S1). As the absorbance of –OH (trough at approximately $3,580 \, cm^{-1}$) for MnO_x-4.5 increased, it became evident that MnO_x-4.5 enhances the formation of carboxylates (e.g., carboxylic acid or hydroperoxides), which tend to accumulate on the surface of TMI and exhibit greater resistance to decomposition than isoprene (Chen et al., 2018; Qu et al., 2022).

As shown in Figure 5e, we propose a GF metric to estimate the nanoparticle growth derived from the IPOOM complexes, which correlates with the increasing intensities of infrared (IR) adsorption observed in the DRIFTS spectra. In response to the evolution of isoprene oxidation (Figure 2a), the GF for the three MnO_x mixtures shows rapid initial increases in organic uptake by the nanoparticles before approaching equilibrium ($\sim$240 min). When isoprene conversion reached equilibrium, the GF values varied: 9.07 for MnO_x-4.5, 8.17 for MnO_x-3.0, and 6.82 for MnO_x-0, indicating that the presence of K^+ enhances organic uptake. Several processes may govern this uptake. The oxidation processes occurring on TMI aerosol surfaces must be rapid to compete with other oxidation pathways and contribute significantly to gas-to-particle conversion (Harris et al., 2013). Low-molecular-weight oxidation products of isoprene tend to chemisorb and become immobilized on the surfaces of MnO_x mixtures, owing to their surface microphysical properties including large specific surface area, microporosity, and strong interfacial interactions through the oxygen-atom binding (shown in Figure 5d). The formation of carboxylates, as observed in Figure 5a–5c, affects the initial stages of particle growth (Li et al., 2021; Riipinen et al., 2012; Wennberg et al., 2018). Following this rapid growth driven by the condensation of organic vapors, organic oligomers and polymers are continuously generated. These compounds can serve as sources of low-volatility organics within the particulate phase, particularly through reactions involving Criegee intermediates and organic acids (Vansco et al., 2020). While there may be reversible partitioning between the condensation and evaporation of IPOOM, the subsequent growth toward equilibrium occurs slowly due to the limited molecular diffusion at the surfaces. The mixing ages of nanoparticles can extend to several hours much slower for liquids, which can constrain further growth (Riipinen et al., 2012). Despite this, surface reactions proceeding at maximum kinetics can still result in the exhaustion or dilution of condensable gases and potential loss of coatings (Sedlacek III et al., 2022). Consequently, the aging MnO_x particles remain highly dynamic throughout the life cycle of nanoparticle growth, reflecting the complex interactions and transformations occurring in the atmosphere.

4. Conclusions and Implications

While the quantitative effects of heterogeneous chemistry remain uncertain, this study presents a condensed framework to illustrate the generation of OH radicals through a TMI pathway, emphasizing the associated surface-enhanced oxidation of isoprene (Figure 6). The chemical interactions among various pollutants are complex under polluted haze conditions (Liu et al., 2022; Lu et al., 2018; Ma et al., 2023). Field observations indicate that Mn exhibits similar temporal patterns to major isoprene oxidation products during winter haze episodes. Additionally, the presence of alkali metal K^+ ions has been correlated with the heterogeneous oxidation of isoprene. Unlike gas-phase oxidation, photosensitized surface-enhanced catalysis by TMI-oxide nanoparticles displays distinct surface-specific profiles, surface ROS generation, and unique interfacial binding modes with reactants. The surface properties of MnO_x mixtures, including specific surface area and microporosity greater than $PM_{2.5}$, act as reservoirs for gas molecule adsorption, thereby prolonging the residence times of reagents. The $^1O_2$ and OH radicals are produced through photoinduced electron energy transfers associated with manganese oxidation-state dismutations coupled with reactions involving oxygen atoms. This study further explores the catalytic role of K^+ mixed with MnO_x in enhancing OH production. The influence of TMI pathways may vary under high ionic strength conditions associated with alkali metals (Wang et al., 2022). The presence of these ions can modify the surface microphysical properties of TMI particles, affecting their ability to absorb water and subsequently impacting the overall reaction dynamics. The resulting OH radicals could diffuse from the surface and contribute to gas-phase oxidation (Chen et al., 2012). However, quantifying the contribution of TMI-catalyzed OH production to the total OH production remains challenging.

The IPOOM complexes are chemisorbed and immobilized on MnO_x surfaces through two types of interfacial binding modes: predominant bidentate (chelating or bridging) and minor monodentate configurations. As the degradation of isoprene, indicated by the loss of oxygen atoms, increases upon interfacial contact with the metals, the OH-initiated oxidation of ISOPOO and ISOPOOH can further decompose into low-molecular-weight
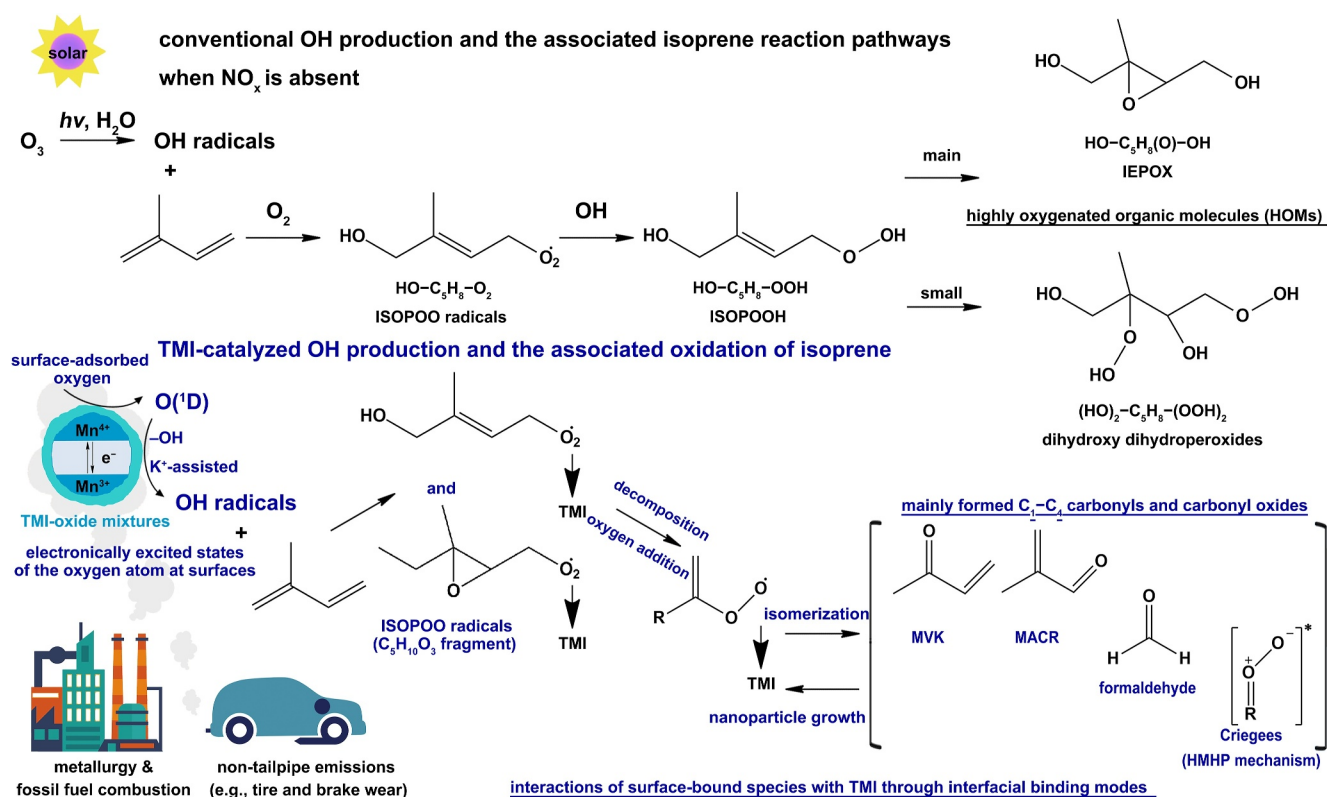
Figure 6. Mechanism for surface-enhanced OH production and heterogeneous reactions of isoprene compared to conventional mechanism.

products. These binding modes facilitate the interaction and mixing between TMI and other aerosol components, which may significantly influence particle growth, air quality, and climate responses (Riipinen et al., 2012). To better understand the heterogeneous reaction rates, these can be normalized by the unit surface area of MnO_x, particularly once isoprene consumption reaches equilibrium. While the atmospheric context may not always allow for strict equilibrium, this normalization simplifies the analysis of molecular diffusion and interfacial mass transport, providing kinetic parameters for modeling heterogeneous dynamics. By incorporating surface-enhanced heterogeneous reactions, the box model results align closely with experimental findings, demonstrating increased kinetics and product yields that surpass those observed in gas-phase reactions of isoprene (Nguyen et al., 2016; Rickard et al., 2015). Despite the experimental design intended to minimize uncertainties related to wall loss and flow dynamics, it is important to note that the uncertainties in estimating heterogeneous reaction rates are greater than those found in field measurements. This discrepancy arises from the limited understanding of the active fraction of TMI aerosol particles. In addition, trace gases such as NO_2 and SO_2 can engage in competitive reactions that consume OH radicals, thereby reducing their availability for other oxidation processes, including the oxidation of isoprene. The subsequent formation of complex aerosol mixtures further influences the reactivity and stability of OH radicals. This adds another layer of complexity to the system. Model predictions constrained by the first-order rate constant for the heterogeneous loss of isoprene under equilibrium conditions introduce further uncertainties (Jacob, 2000; Wang et al., 2022; Wennberg et al., 2018). These complexities highlight the challenges in accurately modeling the dynamics of heterogeneous reactions in atmospheric chemistry.

Conflict of Interest

The authors declare no conflicts of interest relevant to this study.

Data Availability Statements

All data used in this study are available on the website of Figshare (Li et al., 2024).

References

Allen, H. M., Crounse, J. D., Bates, K. H., Teng, A. P., Krawiec-Thayer, M. P., Rivera-Rios, J. C., et al. (2018). Kinetics and product yields of the OH initiated oxidation of hydroxymethyl hydroperoxide. *Journal of Physical Chemistry A*, *122*(30), 6292–6302. https://doi.org/10.1021/acs.jpca.8b04577

Bai, B., & Li, J. (2014). Positive effects of K^+ ions on three-dimensional mesoporous Ag/Co_3O_4 catalyst for HCHO oxidation. *ACS Catalysis*, *4*(8), 2753–2762. https://doi.org/10.1021/cs5006663

Berndt, T., Herrmann, H., Sipil, M., & Kulmala, M. (2016). Highly oxidized second-generation products from the gas-phase reaction of OH radicals with isoprene. *Journal of Physical Chemistry A*, *120*(51), 10150–10159. https://doi.org/10.1021/acs.jpca.6b10987

Bernhammer, A. K., Breitenlechner, M., Keutsch, F. N., & Hansel, A. (2017). Technical note: Conversion of isoprene hydroxy hydroperoxides (ISOPOOHs) on metal environmental simulation chamber walls. *Atmospheric Chemistry and Physics*, *17*(6), 4053–4062. https://doi.org/10.5194/acp-2016-816

Cao, J., Wang, Q., Li, L., Zhang, Y., Tian, J., Chen, L. A., et al. (2020). Evaluation of the oxidation flow reactor for particulate matter emission limit certification. *Atmospheric Environment*, *224*, 117086–117101. https://doi.org/10.1016/j.atmosenv.2019.117086

Chen, H., Nanayakkara, C. E., & Grassian, V. H. (2012). Titanium dioxide photocatalysis in atmospheric chemistry. *Chemical Reviews*, *112*(11), 5919–5948. https://doi.org/10.1021/cr3002092

Chen, Y., Tong, S., Li, W., Liu, Y., Tan, F., Ge, M., et al. (2021). Photocatalytic oxidation of SO_2 by TiO_2: Aerosol formation and the key role of gaseous reactive oxygen species. *Environmental Science & Technology*, *55*(14), 9784–9793. https://doi.org/10.1021/acs.est.1c01608

Chen, Y., Tong, S., Wang, J., Peng, C., Ge, M., Xie, X., & Sun, J. (2018). Effect of titanium dioxide on secondary organic aerosol formation. *Environmental Science & Technology*, *52*(20), 11612–11620. https://doi.org/10.1021/acs.est.8b02466

Chu, B., Chen, T., Liu, Y., Ma, Q., Mu, Y., Wang, Y., et al. (2022). Application of smog chambers in atmospheric process studies. *National Science Review*, *9*(2), nwab103. https://doi.org/10.1093/nsr/nwab103

Chu, B., Wang, Y., Yang, W., Ma, J., He, H., Zhang, P., et al. (2019). Effects of NO_2 and C_3H_6 on the heterogeneous oxidation of SO_2 on TiO_2 in the presence or absence of UV irradiation. *Atmospheric Chemistry and Physics*, *19*, 14777–14790. https://doi.org/10.5194/acp-2019-532

Coggon, M. M., Gkatzelis, G. I., Mcdonald, B. C., Gilman, J. B., Schwantes, R. H., Nader, A., et al. (2021). Volatile chemical product emissions enhance ozone and modulate urban chemistry. *Proceedings of the National Academy of Sciences* (Vol. 118(32), e2026653118). https://doi.org/10.1073/pnas.2026653118

Durand, J. P., Senanayake, S. D., Suib, S. L., & Mullins, D. R. (2010). Reaction of formic acid over amorphous manganese oxide catalytic systems: An in situ study. *Journal of Physical Chemistry C*, *114*(47), 20000–20006. https://doi.org/10.1021/jp104629j

Edwards, P. M., Aikin, K. C., Dube, W. P., Fry, J. L., Gilman, J. B., Gouw, J. D., et al. (2017). Transition from high-to low-NO_x control of night-time oxidation in the southeastern US. *Nature Geoscience*, *10*(7), 490–495. https://doi.org/10.1038/ngeo2976

Franco, B., Blumenstock, T., Cho, C., Clarisse, L., Clerbaux, C., Coheur, P.-F., et al. (2021). Ubiquitous atmospheric production of organic acids mediated by cloud droplets. *Nature*, *593*(7858), 233–237. https://doi.org/10.1038/s41586-021-03462-x

Gao, J., Shi, G., Zhang, Z., Wei, Y., Tian, X., Feng, Y., et al. (2022). Targeting atmospheric oxidants can better reduce sulfate aerosol in China: H_2O_2 aqueous oxidation pathway dominates sulfate formation in haze. *Environmental Science & Technology*, *56*(15), 10608–10618. https://doi.org/10.1021/acs.est.2c01739

George, I., & Abbatt, J. (2010). Heterogeneous oxidation of atmospheric aerosol particles by gas-phase radicals. *Nature Chemistry*, *2*(9), 713–722. https://doi.org/10.1038/nchem.806

Harris, E., Sinha, B., Foley, S., Crowley, J. N., Borrmann, S., & Hoppe, P. (2012). Sulfur isotope fractionation during heterogeneous oxidation of SO_2 on mineral dust. *Atmospheric Chemistry and Physics*, *12*(11), 4867–4884. https://doi.org/10.5194/acp-12-4867-2012

Harris, E., Sinha, B., Van Pinxteren, D., Tilgner, A., Fomba, K. W., Schneider, J., et al. (2013). Enhanced role of transition metal ion catalysis during in-cloud oxidation of SO_2. *Science*, *340*(6133), 727–730. https://doi.org/10.1126/science.1230911

He, G., Ma, J., Chu, B., Hu, R., Li, H., Gao, M., et al. (2022). Generation and release of OH radicals from the reaction of H_2O with O_2 over soot. *Angewandte Chemie*, *134*(21), e202201638. https://doi.org/10.1002/anie.202201638

Hochella, M. F., Mogk, D. W., Ranville, J., Allen, I. C., Luther, G. W., Marr, L. C., et al. (2019). Natural, incidental, and engineered nanomaterials and their impacts on the Earth system. *Science*, *363*(6434), 1414–1423. https://doi.org/10.1126/science.aau8299

Jacob, D. J. (2000). Heterogeneous chemistry and tropospheric ozone. *Atmospheric Environment*, *34*(12–14), 2131–2159. https://doi.org/10.1016/S1352-2310(99)00462-8

Jaoui, M., Szmigielski, R., Nestorowicz, K., Kolodziejczyk, A., Sarang, K., Rudzinski, K. J., et al. (2019). Organic hydroxy acids as Highly Oxygenated Molecular (HOM) tracers for aged isoprene aerosol. *Environmental Science & Technology*, *53*(24), 14516–14527. https://doi.org/10.1021/acs.est.9b05075

Jia, X., Ma, J., Xia, F., Xu, Y., Gao, J., & Xu, J. (2018). Carboxylic acid-modified metal oxide catalyst for selectivity-tunable aerobic ammoxidation. *Nature Communications*, *9*(1), 933–939. https://doi.org/10.1038/s41467-018-03358-x

Keller, A. A., Mcferran, S., Lazareva, A., & Suh, S. (2013). Global life cycle releases of engineered nanomaterials. *Journal of Nanoparticle Research*, *15*(6), 1692–1708. https://doi.org/10.1007/s11051-013-1692-4

Kong, X., Castarède, D., Thomson, E. S., Boucly, A., Artiglia, L., Ammann, M., et al. (2021). A surface-promoted redox reaction occurs spontaneously on solvating inorganic aerosol surfaces. *Science*, *374*(6568), 747–752. https://doi.org/10.1126/science.abc5311

Li, H., Cui, L., Lu, Y., Huang, Y., Cao, J.-j., Park, D., et al. (2019). In situ intermediates determination and cytotoxicological assessment in catalytic oxidation of formaldehyde: Implications for catalyst design and selectivity enhancement under ambient conditions. *Environmental Science & Technology*, *53*(9), 5230–5240. https://doi.org/10.1021/acs.est.8b06234

Li, H., Li, J., Ho, W., Cui, L., Wang, M., Zhang, Y., et al. (2024). Data 2024JD042439.xlsx [Dataset]. *Figshare*. https://doi.org/10.6084/m9.figshare.27999305

Li, H., Wang, D., Cui, L., Gao, Y., Huo, J., Wang, X., et al. (2019). Characteristics of atmospheric $PM_{2.5}$ composition during the implementation of stringent pollution control measures in Shanghai for the 2016 G20 summit. *Science of the Total Environment*, *648*, 1121–1129. https://doi.org/10.1016/j.scitotenv.2018.08.219

Li, J., Zhang, Y., Cao, F., Zhang, W., Michalski, G., & Lee, X. (2020). Stable sulfur isotopes revealed a major role of transition-metal-ion catalyzed SO_2 oxidation in haze episodes. *Environmental Science & Technology*, *54*(5), 2626–2634. https://doi.org/10.1021/acs.est.9b07150

Li, K., Guo, Y., Nizkorodov, S. A., Rudich, Y., Angelaki, M., Wang, X., et al. (2023). Spontaneous dark formation of OH radicals at the interface of aqueous atmospheric droplets. *Proceedings of the National Academy of Sciences* (Vol. 120(15), e2220228120). https://doi.org/10.1073/pnas.2220228120

Li, Y., Zhao, J., Wang, Y., Seinfeld, J. H., & Zhang, R. (2021). Multigeneration production of secondary organic aerosol from toluene photo-oxidation. *Environmental Science & Technology*, *55*(13), 8592–8603. https://doi.org/10.1021/acs.est.1c02026

Liu, Y., He, G., Chu, B., Ma, Q., & He, H. (2022). Atmospheric heterogeneous reactions on soot: A review. *Fundamental Research*, *3*(4), 579–591. https://doi.org/10.1016/j.fmre.2022.02.012

Lu, K., Guo, S., Tan, Z., Wang, H., Zhang, Y., Liu, Y., et al. (2018). Exploring the atmospheric free radical chemistry in China: The self-cleansing capacity and the formation of secondary air pollution. *National Science Review*, *6*(3), 579–594. https://doi.org/10.1093/nsr/nwy073

Ma, Q., Zhang, C., Liu, C., He, G., Zhang, P., Li, H., et al. (2023). A review on the heterogeneous oxidation of SO_2 on solid atmospheric particles: Implications for sulfate formation in haze chemistry. *Critical Reviews in Environmental Science and Technology*, *53*(21), 1888–1911. https://doi.org/10.1080/10643389.2023.2190315

Manfrin, A., Nizkorodov, S. A., Malecha, K. T., Getzinger, G. J., McNeill, K., & Borduas-Dedekind, N. (2019). Reactive oxygen species production from secondary organic aerosols: The importance of singlet oxygen. *Environmental Science & Technology*, *53*(15), 8553–8562. https://doi.org/10.1021/acs.est.9b01609

McFiggans, G., Mentel, T. F., Wildt, J., Pullinen, I., Kang, S., Kleist, E., et al. (2019). Secondary organic aerosol reduced by mixture of atmospheric vapours. *Nature*, *565*(7741), 587–593. https://doi.org/10.1038/s41586-018-0871-y

Müller, J., Peeters, J., & Stavrakou, T. (2014). Fast photolysis of carbonyl nitrates from isoprene. *Atmospheric Chemistry and Physics*, *14*(11), 31127–31159. https://doi.org/10.5194/acp-14-2497-2014

Ndour, M., Conchon, P., D'Anna, B., Ka, O., & George, C. (2009). Photochemistry of mineral dust surface as a potential atmospheric renoxification process. *Geophysical Research Letters*, *36*(5), L05816. https://doi.org/10.1029/2008gl036662

Nguyen, T. B., Tyndall, G. S., Crounse, J. D., Teng, A. P., Bates, K. H., Schwantes, R. H., et al. (2016). Atmospheric fates of Criegee intermediates in the ozonolysis of isoprene. *Physical Chemistry Chemical Physics*, *18*(15), 10241–10254. https://doi.org/10.1039/c6cp00053c

Nie, L., Yu, J., Li, X., Cheng, B., Liu, G., & Jaroniec, M. (2013). Enhanced performance of NaOH-modified Pt/TiO_2 toward room temperature selective oxidation of formaldehyde. *Environmental Science & Technology*, *47*(6), 2777–2783. https://doi.org/10.1021/es3045949

Nosaka, Y., & Nosaka, A. Y. (2017). Generation and detection of reactive oxygen species in photocatalysis. *Chemical Reviews*, *117*(17), 11302–11336. https://doi.org/10.1021/acs.chemrev.7b00161

Paulot, F., Crounse, J. D., Kjaergaard, H. G., Kroll, J. H., Seinfeld, J. H., & Wennberg, P. O. (2009). Isoprene photooxidation: New insights into the production of acids and organic nitrates. *Atmospheric Chemistry and Physics*, *9*(4), 1479–1501. https://doi.org/10.5194/acp-9-1479-2009

Paulot, F., Crounse, J. D., Kjaergaard, H. G., Kürten, A., St. Clair, J. M., Seinfeld, J. H., & Wennberg, P. O. (2009). Unexpected epoxide formation in the gas-phase photooxidation of isoprene. *Science*, *325*(5941), 730–733. https://doi.org/10.1126/science.1172910

Qu, W., Tang, Z., Liu, W., Liao, Y., Huang, Y., Xia, D., et al. (2022). Self-accelerating interfacial catalytic elimination of gaseous sulfur-containing volatile organic compounds as microbubbles in a facet-engineered three-dimensional BiOCl sponge Fenton-like process. *Environmental Science & Technology*, *56*(16), 11657–11669. https://doi.org/10.1021/acs.est.2c01798

Quiroz, J., Giraudon, J. M., Gervasini, A., Dujardin, C., Lancelot, C., Trentesaux, M., & Lamonier, J. F. (2015). Total oxidation of formaldehyde over MnO_x–CeO_2 catalysts: The effect of acid treatment. *ACS Catalysis*, *5*(4), 2260–2269. https://doi.org/10.1021/cs501879j

Rickard, A. R., Jenkin, M. E., et al. (2015). The MCM v3.3.1 degradation scheme for isoprene. *Atmospheric Chemistry and Physics*, *15*(20), 11433–11459. https://doi.org/10.5194/acp-15-11433-2015

Riipinen, I., Yli-Juuti, T., Pierce, J. R., Petäjä, T., Worsnop, D. R., Kulmala, M., & Donahue, N. M. (2012). The contribution of organics to atmospheric nanoparticle growth. *Nature Geoscience*, *5*(7), 453–458. https://doi.org/10.1038/ngeo1499

Rivera-Rios, J. C., Nguyen, T. B., Crounse, J. D., Jud, W., St. Clair, J. M., Mikoviny, T., et al. (2015). Conversion of hydroperoxides to carbonyls in field and laboratory instrumentation: Observational bias in diagnosing pristine versus anthropogenically controlled atmospheric chemistry. *Geophysical Research Letters*, *41*(23), 8645–8651. https://doi.org/10.1002/2014GL061919

Schweitzer, C., & Schmidt, R. (2003). Physical mechanisms of generation and deactivation of singlet oxygen. *Chemical Reviews*, *103*(5), 1685–1758. https://doi.org/10.1021/cr010371d

Sedlacek III, A. J., Lewis, E. R., Onasch, T. B., Zuidema, P., Redemann, J., Jaffe, D., & Kleinman, L. I. (2022). Using the black carbon particle mixing state to characterize the lifecycle of biomass burning aerosols. *Environmental Science & Technology*, *56*(20), 14315–14325. https://doi.org/10.1021/acs.est.2c03851

Seinfeld, J. H., & Pandis, S. N. (2016). *Atmospheric chemistry and physics: From air pollution to climate change* (3rd ed.). John Wiley and Sons, Inc.1152.

Shen, H., Vereecken, L., Kang, S., Pullinen, I., Fuchs, H., Zhao, D., & Mentel, T. F. (2022). Unexpected significance of a minor reaction pathway in daytime formation of biogenic highly oxygenated organic compounds. *Science Advances*, *8*(42), eabp8702. https://doi.org/10.1126/sciadv.abp8702

Singh, S. P. (2021). Quantum chemical study of gas-phase reactions of isoprene with OH radicals producing highly oxidised second-generation products. *Journal of Molecular Modeling*, *27*, 1–10. https://doi.org/10.1007/s00894-021-04666-8

Song, H., Lu, K., Ye, C., Dong, H., Li, S., Chen, S., et al. (2021). A comprehensive observation-based multiphase chemical model analysis of sulfur dioxide oxidations in both summer and winter. *Atmospheric Chemistry and Physics*, *21*(17), 13713–13727. https://doi.org/10.5194/acp-21-13713-2021

Urupina, D., Gaudion, V., Romanias, M. N., & Thevenet, F. (2022). Surface distribution of sulfites and sulfates on natural volcanic and desert dusts: Impact of humidity and chemical composition. *ACS Earth and Space Chemistry*, *6*(3), 642–655. https://doi.org/10.1021/acsearthspacechem.1c00321

Vansco, M. F., Caravan, R. L., Pandit, S., Zuraski, K., Winiberg, F. A., Au, K., et al. (2020). Formic acid catalyzed isomerization and adduct formation of an isoprene-derived Criegee intermediate: Experiment and theory. *Physical Chemistry Chemical Physics*, *22*(46), 26796–26805. https://doi.org/10.1039/d0cp05018k

Wang, D., & Didier, A. (2017). The recent development of efficient Earth-abundant transition-metal nanocatalysts. *Chemical Society Reviews*, *46*(3), 816–854. https://doi.org/10.1039/c6cs00629a

Wang, J., Li, J., Jiang, C., Zhou, P., Zhang, P., & Yu, J. (2017). The effect of manganese vacancy in birnessite-type MnO_2 on room-temperature oxidation of formaldehyde in air. *Applied Catalysis B: Environmental*, *204*, 147–155. https://doi.org/10.1016/j.apcatb.2016.11.036

Wang, J., Zhang, P., Li, J., Jiang, C., Yunus, R., & Kim, J. (2015). Room-temperature oxidation of formaldehyde by layered manganese oxide: Effect of water. *Environmental Science & Technology*, *49*(20), 12372–12379. https://doi.org/10.1021/acs.est.5b02085

Wang, T., Liu, Y. Y., Cheng, H. Y., Wang, Z. Z., Fu, H. B., Chen, J. M., & Zhang, L. (2022). Significant formation of sulfate aerosols contributed by the heterogeneous drivers of dust surface. *Atmospheric Chemistry and Physics*, *22*(20), 13467–13493. https://doi.org/10.5194/acp-22-13467-2022

Wang, W., Liu, M., Wang, T., Song, Y., Ge, M., Cao, J., et al. (2021). Sulfate formation is dominated by manganese-catalyzed oxidation of SO_2 on aerosol surfaces during haze events. *Nature Communications*, *12*(1), 1993–2002. https://doi.org/10.1038/s41467-021-22091-6

Welz, O., Savee, J. D., Osborn, D. L., Vasu, S. S., Percival, C. J., Shallcross, D. E., & Taatjes, C. A. (2012). Direct kinetic measurements of Criegee intermediate (CH_2OO) formed by reaction of CH_2I with O_2. *Science*, *335*(6065), 204–207. https://doi.org/10.1126/science.1213229

Wennberg, P. O., Bates, K. H., Crounse, J. D., Dodson, L. G., Mcvay, R. C., Mertens, L. A., et al. (2018). Gas-phase reactions of isoprene and its major oxidation products. *Chemical Reviews*, *118*(7), 3337–3390. https://doi.org/10.1021/acs.chemrev.7b00439

Xu, H., Yan, N., Qu, Z., Liu, W., Mei, J., Huang, W., & Zhao, S. (2017). Gaseous heterogeneous catalytic reactions over Mn-based oxides for environmental applications: A critical review. *Environmental Science & Technology*, *51*(16), 8879–8892. https://doi.org/10.1021/acs.est.6b06079

Xu, Z. N., Nie, W., Chi, X. G., Sun, P., Huang, D. D., Yan, C., et al. (2021). Multifunctional products of isoprene oxidation in polluted atmosphere and their contribution to SOA. *Geophysical Research Letters*, *48*(1), e2020GL089276. https://doi.org/10.1029/2020GL089276

Yuan, B., Koss, A. R., Warneke, C., Coggon, M., Sekimoto, K., & Gouw, J. D. (2017). Proton-transfer-reaction mass spectrometry: Applications in atmospheric sciences. *Chemical Reviews*, *117*(21), 13187–13229. https://doi.org/10.1021/acs.chemrev.7b00325

Yu-Te, S., Yu-Hsuan, H., A, W. H., & Yuan-Pern, L. (2013). Infrared absorption spectrum of the simplest Criegee intermediate CH_2OO. *Science*, *340*(6129), 174–176. https://doi.org/10.1126/science.1234369

Zhang, P., Chen, T., Ma, Q., Chu, B., Wang, Y., Mu, Y., et al. (2022). Diesel soot photooxidation enhances the heterogeneous formation of H_2SO_4. *Nature Communications*, *13*(1), 1–9. https://doi.org/10.1038/s41467-022-33120-3

Zhu, S., Zhou, M., Qiao, L., Huang, D. D., Wang, Q., Wang, S., et al. (2023). Evolution and chemical characteristics of organic aerosols during wintertime $PM_{2.5}$ episodes in Shanghai, China: Insights gained from online measurements of organic molecular markers. *Atmospheric Chemistry and Physics*, *23*(13), 7551–7568. https://doi.org/10.5194/acp-23-7551-2023

References From the Supporting Information

Coggon, M. M., Stockwell, C. E., Claflin, M. S., Pfannerstill, E. Y., Xu, L., Gilman, J. B., et al. (2024). Identifying and correcting interferences to PTR-ToF-MS measurements of isoprene and other urban volatile organic compounds. *Atmospheric Measurement Techniques*, *17*(2), 801–825. https://doi.org/10.5194/amt-17-801-2024

Dagher, Z., Garon, G., Billet, S., Gosset, P., Shirali, P., Courcot, D., et al. (2006). Activation of different pathways of apoptosis by air pollution particulate matter ($PM_{2.5}$) in human epithelial lung cells (L132) in culture. *Toxicology*, *225*(1), 12–24. https://doi.org/10.1016/j.tox.2006.04.038

Eisfeld, W., & Francisco, J. S. (2008). Excited states and photodissociation of hydroxymethyl hydroperoxide. *Journal of Physical Chemistry*, *128*(17), 174304–174310. https://doi.org/10.1063/1.2909547

Ervens, B., & Volkamer, R. (2010). Glyoxal processing by aerosol multiphase chemistry: Towards a kinetic modeling framework of secondary organic aerosol formation in aqueous particles. *Atmospheric Chemistry and Physics*, *10*(17), 8219–8244. https://doi.org/10.5194/acp-10-8219-2010

Gomez-Moreno, F. J., Pujadas, M., Plaza, J., Rodriguez-Maroto, J. J., Martinez-Lozano, P., & Artinano, B. (2011). Influence of seasonal factors on the atmospheric particle number concentration and size distribution in Madrid. *Atmospheric Environment*, *45*(18), 3169–3180. https://doi.org/10.1016/j.atmosenv.2011.02.041

Hu, M., Liu, S., Wu, Z.-j., Zhang, J., Zhao, Y., Wehner, B., et al. (2006). Effects of high temperature, high relative humidity and rain process on particle size distributions in summer of Beijing. *Environmental Sciences*, *27*(11), 2293–2298. https://doi.org/10.3321/j.issn:0250-3301.2006.11.028

Hussein, T., Puustinen, A., Aalto, P. P., Mäkelä, J. M., Hämeri, K., & Kulmala, M. (2003). Urban aerosol number size distributions. *Atmospheric Chemistry and Physics*, *3*(5), 391–411. https://doi.org/10.5194/acp-4-391-2004

Li, H., Ho, W. K., Cao, J. J., Park, D., & Huang, Y. (2019). Active complexes on engineered crystal facets of MnO_x–CeO_2 and scale-up demonstration on an air cleaner for indoor formaldehyde removal. *Environmental Science & Technology*, *53*(18), 10906–10916. https://doi.org/10.1021/acs.est.9b03197

Li, H., Huang, T., Lu, Y., Cui, L., Wang, Z., Zhang, C., et al. (2018). Unraveling the mechanisms of room-temperature catalytic degradation of indoor formaldehyde and its biocompatibility on colloidal TiO_2-supported MnO_x–CeO_2. *Environmental Science: Nano*, *5*(5), 1130–1139. https://doi.org/10.1039/c8en00176f

Liao, L.-F., Lien, C.-F., & Lin, J.-L. (2001). FTIR study of adsorption and photoreactions of acetic acid on TiO_2. *Physical Chemistry Chemical Physics*, *3*(17), 3831–3837. https://doi.org/10.1039/B103419G

Longley, I. D., Gallagher, M. W., Dorsey, J. R., Flynn, M., Inglis, D., & Alfarra, M. (2003). A case study of aerosol (4.6 nm < Dp < 10 μm) number and mass size distribution measurements in a busy street canyon in Manchester, UK. *Atmospheric Environment*, *37*(12), 1563–1571. https://doi.org/10.1016/S1352-2310(03)00010-4

Lu, Y., Chen, M., Huang, T., Huang, Y., Cao, J. J., Li, H. W., et al. (2021). Oxygen vacancy-dependent photocatalytic activity of well-defined $Bi_2Sn_2O_{7-x}$ hollow nanocubes on NO_x removal. *Environmental Science: Nano*, *8*(7), 1927–1933. https://doi.org/10.1039/d1en00260k

Roehl, C. M., Marka, Z., Fry, J. L., & Wennberg, P. O. (2007). Near-UV photolysis cross sections of CH_3OOH and $HOCH_2OOH$ determined via action spectroscopy. *Atmospheric Chemistry and Physics*, *7*(3), 713–720. https://doi.org/10.5194/acp-7-713-2007

Rosales, C. M. F., Jiang, J., Lahib, A., Bottorff, B. P., Reidy, E. K., Kumar, V., et al. (2022). Chemistry and human exposure implications of secondary organic aerosol production from indoor terpene ozonolysis. *Science Advances*, *8*(8), eabj9156. https://doi.org/10.1126/sciadv.abj9156

Selvakumar, S., Nuns, N., Trentesaux, M., Batra, V., Giraudon, J.-M., & Lamonier, J.-F. (2018). Reaction of formaldehyde over birnessite catalyst: A combined XPS and ToF-SIMS study. *Applied Catalysis B: Environmental*, *223*, 192–200. https://doi.org/10.1016/j.apcatb.2017.05.029

Stanier, C. O., Khlystov, A. Y., & Pandis, S. N. (2004). Ambient aerosol size distributions and number concentrations measured during the Pittsburgh Air Quality Study (PAQS). *Atmospheric Environment*, *38*(20), 3275–3284. https://doi.org/10.1016/j.atmosenv.2004.03.020

Wang, X., Liu, T., Bernard, F., Ding, X., Wen, S., Zhang, Y., et al. (2014a). Design and characterization of a smog chamber for studying gas-phase chemical mechanisms and aerosol formation. *Atmospheric Measurement Techniques*, *7*(1), 301–313. https://doi.org/10.5194/amt-7-301-2014

Wang, Y., Zhu, X., Crocker, M., Chen, B., & Shi, C. (2014b). A comparative study of the catalytic oxidation of HCHO and CO over $Mn_{0.75}Co_{2.25}O_4$ catalyst: The effect of moisture. *Applied Catalysis B: Environmental*, *160*, 542–551. https://doi.org/10.1016/j.apcatb.2014.06.011